The governing factors controlling the leaching behaviour of PFAS-compounds from the unsaturated zone to groundwater: an analysis using a scenario-based modelling approach.

A thesis presented in partial fulfilment of the requirements for the degree of

Master of Science

Author:
Hugo van den Berg, BSc.[a]

Supervisors:
dr. ing. Johan van Leeuwen[b,a]
dr. Niels Hartog[a,b]

4 June 2023

[a] Department of Earth Sciences, Faculty of Geosciences, Utrecht University
[b] KWR Water Research Institute

Contents

Abstract

Per- and polyfluoroalkyl substances (PFASs) have attracted attention for their widespread occurrence in the environment, combined with their high mobility and bioaccumulation potential. PFASs deposited on land surfaces are first transported through the unsaturated zone, where adsorption to both solid-water interfaces (SWIs) and air-water interfaces (AWIs) is expected to occur. In order to ensure that the concentration of PFAS in drinking water wells is sufficiently low to comply with strict regulations, a thorough understanding of these transport processes in the subsurface is necessary. This study uses an analytical solution to the advection-dispersion equation to perform numerical simulations of the transport of PFAS in the unsaturated zone in Dutch soils, under average Dutch climate conditions. The results show that the leaching of PFAS is fastest for short chained PFASs, and decreases in transport velocity with increasing chain length. For short chained PFASs the retardation factor is small (average per simulated soil for TFA: $R = 1.05$ to 1.34), and the transport velocity is mostly similar to the water velocity. For long chained PFASs the retardation factor is large (average per simulated soil for PFDA: $R = 33.3$ to 645), and the transport velocity is mostly governed by sorption, especially to AWIs, but also to SWIs. The results also show that the leaching of long chained PFAS from the unsaturated zone is relatively faster in clayey soils, which have the highest water saturation, and therefore the smallest air-water interfacial area (A_{aw}). Most important uncertainties remain in the value of A_{aw} due to a lack of measurements in Dutch soils, but also due to the steady-state approach of this study which does not account for temporal variability in water saturation and consequently in the value of A_{aw}. Another source of uncertainty regarding the expected breakthrough and concentration in drinking water wells is the lack of data in the historical use and deposition of PFASs in the Netherlands.

List of Figures

List of Tables

Chapter 1

Introduction

Per- and polyfluoroalkyl substances (PFASs) are synthetic substances that were first designed in the 1930s and 1940s for their chemical stability and their influence on surface tension (Krafft & Riess, 2015). The surface-active properties are caused by the contrast between the hydrophobic tail of CF_x groups and the hydrophilic head of the molecule. These substances are used in a wide variety of applications, such as fire-fighting foams, lubricants, and water- and oil repellent coatings. Significant volumes are released into the environment, both through direct release from fire-fighting foams, and through indirect losses during the use and disposal of consumer goods. (Paul et al., 2008)

Due to their widespread application and high mobility, PFAS are found in all compartments of the environment, even in remote locations such as the polar regions (Alfaro Garcia et al., 2022). They have attracted attention for their bioaccumulation potential, and several PFASs are included in a risk assessment by the European Food Safety Authority (EFSA) that advises a tolerable weekly intake of only 4.4 $ng/kg_{bodyweight}$ (EFSA Panel on Contaminants in the Food Chain et al., 2020). In order to compare the risk of different PFASs, the National Institute for Public Health and the Environment (RIVM) in the Netherlands has developed a relative potential factor (RPF) comparing the toxicity of each PFAS to that of perfluorooctanoic acid (PFOA) (Bil et al., 2020). By multiplying the concentration of each PFAS by their respective RPF, a PFOA equivalent concentration (PEQ) is obtained. The RIVM has determined a provisional limit for drinking water of 4.4 ng PEQ/L for the summed concentrations of PFASs. 10 % of all samples from drinking water sourced from groundwater in the Netherlands contain PFASs exceeding this provisional limit (Van der Aa et al., 2022).

In order to ensure that the concentration of PFAS in groundwater wells for drinking water production is sufficiently low to comply with such strict regulations, a thorough understanding of the transport processes in the subsurface is necessary. PFASs deposited on land surfaces are transported through the unsaturated zone to the groundwater. The collection and analysis of high resolution soil moisture samples is both difficult and expensive, making direct observations of the transport of PFASs in the subsurface infeasible. Therefore, the understanding of the processes

is based on models (De Gruijter et al., 2006). To design meaningful laboratory and field experiments for validation of these models, it is necessary to understand the influence of each model parameter on the model outputs, such that these parameters can be accounted for in the experiments.

1.1 Transport of PFAS in the unsaturated zone

The vertical flow of water in the unsaturated zone is described using Darcy's equation:

$$q = -K_{rel}\frac{\partial h}{\partial z}, \tag{1.1}$$

where q is the infiltration flux, K_{rel} is the relative hydraulic conductivity, and $\frac{\partial h}{\partial z}$ is the pressure gradient in the vertical direction. K_{rel} is a function of the soil moisture content, often described using the Van Genuchten-Mualem model (Vereecken et al., 2010):

$$K_{rel}(S) = K_s\, S_w^{\lambda}\left[1-\left(1-S_w^{n/(n-1)}\right)^{(1-1/n)}\right]^2, \tag{1.2}$$

where K_s is the saturated hydraulic conductivity, λ and n are shape parameters, and S_w is the effective saturation as a fraction of the range between the residual and saturated soil moisture content (θ_r and θ_s, respectively):

$$S_w = \frac{\theta-\theta_r}{\theta_s-\theta_r} = \left[1-|\alpha h|^n\right]^{-m}, \tag{1.3}$$

where α is the inverse of the air entry value, and m is another shape parameter, defined as $m = 1-1/n$. (Vereecken et al., 2010)

Solute transport in the unsaturated zone is a combination of advection with the water flow, hydrodynamic dispersion and diffusion, sorption, and chemical reactions. Due to the chemical stability of PFASs, the reaction term can be discarded. Sorption to the SWIs is important for PFASs, especially to organic matter (Fabregat-Palau et al., 2021; Le et al., 2021). On top of that PFASs are also sorbed to air-water interfaces (AWIs), due to the contrast between the hydrophobic tail of CF_x groups and the hydrophilic head of the molecule. (Guo et al., 2020; Silva et al., 2021; Silva et al., 2022).

Adsorption of PFASs to solid-water interfaces is governed by the same equations as for conventional soil contaminations:

$$C_s = K_d\left(C_{aq}\right)\cdot C_{aq}, \tag{1.4}$$

with $K_d\left(C_{aq}\right)$ representing the adsorption isotherm as a function of the aqueous concentration C_{aq}. Sorption to the AWIs follows an equation similar to Equation 1.4

(see also Appendix B), with the exception that the A_{aw} per unit volume of soil has to be included explicitly:

$$C_{aw} = A_{aw}(\theta) \cdot \Gamma_{aw}(C_{aq}) = A_{aw}(\theta) \cdot K_{aw}(C_{aq}) \cdot C_{aq}. \tag{1.5}$$

Determining the A_{aw} is a difficult task, with different measurement techniques resulting in different values (Brusseau & Guo, 2021; Silva et al., 2022). Estimating A_{aw} is possible using the Leverett thermodynamic model (LTM) (Guo et al., 2022; Leverett, 1941):

$$A_{aw} = \frac{\phi}{\sigma} \int_{S_w}^{1} p_c(S_w)\, dS_w\,, \tag{1.6}$$

with ϕ the porosity, σ the surface tension of water, and p_c the capillary pressure at effective saturation S_w. The estimates from the LTM do not match measurements of A_{aw}, especially for soils with a large fraction of fine grains, which can in part be explained by the surface roughness of soil particles (Jiang et al., 2020; Silva et al., 2022). Empirical values for the Surface Roughness Multiplier (SRM) required to fit the measurements are in the order of magnitude of 3 to 4 for natural soils (Guo et al., 2022; Silva et al., 2022), although the values reported by Silva et al. (2022) are not reproducible using the method described in their paper (see also Appendix C).

In contrast to SWIs, where different soil minerals and organic matter each have their own sorption isotherms, AWIs are characterized by a single type of sorption site, which makes adsorption to AWIs follow a single Langmuir isotherm (Guo et al., 2022; Rosen, 2004; Langmuir, 1918):

$$C_{aw} = A_{aw} \cdot \Gamma_{max} \cdot \frac{\kappa_{aw}}{1 + \kappa_{aw} C_{aq}} \cdot C_{aq}, \tag{1.7}$$

where Γ_{max} is the maximum surface excess concentration, and κ_{aw} is the equilibrium constant. As the gas phase provides space for the hydrophobic tail of the PFAS molecules to extend out from the water (Krafft & Riess, 2015), the affinity of various PFASs with the AWI is largely determined by the hydrophobicity of that tail, and thus the number of CF_x groups in the molecule, relative to the hydrophilicity of the head group (Le et al., 2021). As the surface becomes more saturated with PFAS molecules, the electrostatic repulsion between the hydrophilic heads increases. However, in the presence of other dissolved ions in the pore water, this repulsion is decreased, thus increasing Γ_{max} (Rosen, 2004).

Combining the partitioning coefficients for both the solid phase and AWI sorption results in a single retardation factor similar to those calculated for conventional advective flow (Guo et al., 2022):

$$R = 1 + \frac{\rho_b\, K_d}{\theta} + \frac{A_{aw} K_{aw}}{\theta} = 1 + R_s + R_{aw}. \tag{1.8}$$

The transport equations can be solved using numerical solvers, which discretize the model domain in space and time, and solve the equations for each discrete step.

The major advantage of numerical modelling is the flexibility in the discretization, which allows for variations in the model parameters along all model dimensions. This also means that the setup of such models is relatively complex. For PFAS transport in the unsaturated zone an extension to the HYDRUS model code was developed (Silva et al., 2019).

Alternatively, analytical solutions can be used to solve the transport equations. These solutions are based on assumptions of boundary conditions and initial conditions, and are therefore only valid for specific conditions. This does leave a relatively simple model, which requires less input data than a numerical model, and is often faster to run. Guo et al. (2022) developed an analytical solution for PFAS transport in the unsaturated zone.

Most of the work on PFAS transport in the unsaturated zone has been done on laboratory sands such as Accusand, and on American soils (e.g. Guo et al., 2022; Silva et al., 2019). These soils typically contain very little organic matter (Wang et al., 2021). Dutch soils on the other hand are usually richer in organic matter (Heinen et al., 2020). Also, the groundwater recharge flux in the Netherlands is larger than in the US: where Guo et al. (2022) uses a recharge flux of 240 mm/year, the Dutch average recharge is 300 mm/year (Massop et al., 2005). The goal of this research is to investigate the leaching behaviour of PFASs in the Dutch model soils from the Staring series (Heinen et al., 2020). The focus is on dilute concentrations in the order of magnitude of the limits as specified in the drinking water regulations.

Chapter 2

Methods

To describe the leaching behaviour of PFASs in the vadose zone the analytical model by Guo et al. (2022) was selected. This was done because the model source code was available as Python scripts, and provides sufficient flexibility for the research. The analytical solution to the transport equations assumes only steady-state vertical flow with a unit gradient in a semi-infinite unsaturated zone; instantaneous linear equilibrium sorption to air-water interfaces; optionally kinetic, reversible linear sorption to solid-water interfaces; and a pulse injection of PFAS.

As the model code by Guo et al. (2022) does no validation of unit compatibility, a wrapper was written that makes use of the pint package for Python (Grecco, 2022). This wrapping code also groups related parameters into containers, in a way that allows for easy exchange of the main components, such as running the same simulation with different PFASs or different sorption models (Figure 2.1). The source code for this wrapper is available online (Lapré, 2023).

Using this model code, numerical experiments were done simulating soil columns that contain a single soil from the Staring series (Heinen et al., 2020), in which a single PFAS was injected for 25 year at a constant rate of 300 mm/year, equal to the average groundwater recharge in The Netherlands (Massop et al., 2005), and a constant concentration of 1 pmol/L, after which the soil was flushed with clean water for another 225 year to assess how long different soils leach to the groundwater after the input is stopped. This was then done for all combinations of the 18 bottom soil classes from the Staring series and Accusand as a reference, and 12 different PFAS compounds (Table 2.1). The PFAS compounds were selected based on the availability of their physical and chemical properties in the literature, such as Fabregat-Palau et al. (2021) and Guo et al. (2022), or the attention they receive in the media, such as trifluoroacetic acid (TFA) and hexafluoropropylene oxide dimer acid (HFPO-DA). The concentration of 1 pmol/L corresponds to approximately 10 % of the drinking water limit for PFOA, and approximately equal to the drinking water limit for perfluorononanoic acid (PFNA) and perfluorodecanoic acid (PFDA), which have an RPF of 10 (Bil et al., 2020, Table 2.1).

The soil parameters of the Dutch soils were taken from the Staring series (Heinen et al., 2020), which describes the soil water retention curves using the

Table 2.1: Selected PFASs for the numerical experiments.

PFAS	Tail length	Molar mass / g/mol	K_{oc}[a] / L/kg	K_{sc}[a] / L/kg	D_0[b] / 10^{-6} cm²/s	RPF[c] / -
trifluoroacetic acid (TFA)	1	114.02				
perfluorobutanoic acid (PFBA)	3	214.0	2.9	0.43		0.05
perfluorobutane sulfonic acid (PFBS)	4	300.1	11.0	0.44	11	0.001
perfluoropentanoic acid (PFPeA)	4	264.05	15.0	0.46	12	0.05
perfluorohexanoic acid (PFHxA)	5	314.05	15.0	0.46	7.8	0.01
perfluorohexane sulfonic acid (PFHxS)	6	400.12	50.0	1.2	4.5	0.6
perfluoroheptanoic acid (PFHpA)	6	364.06	50.0		9.3	1
perfluorooctanoic acid (PFOA)	7	414.07	107.0	3.3	4.9	1
perfluorooctane sulfonic acid (PFOS)	8	500.13	609.0	9.4	5.4	2
perfluorononanoic acid (PFNA)	8	464.08	324.0	2.0	2.93	10
perfluorodecanoic acid (PFDA)	9	514.08	604.0	14.0	2.27	10
hexafluoropropylene oxide dimer acid (HFPO-DA)	5	330.05				0.06

[a]Values for K_{oc} and K_{sc} are taken from Fabregat-Palau et al. (2021) when available.
[b]Values for D_0 are taken from Guo et al. (2022) when available.
[c]Relative Potency Factors (RPF) are taken from Bil et al. (2020) when available, where ranges were reported only the upper boundary is presented here.

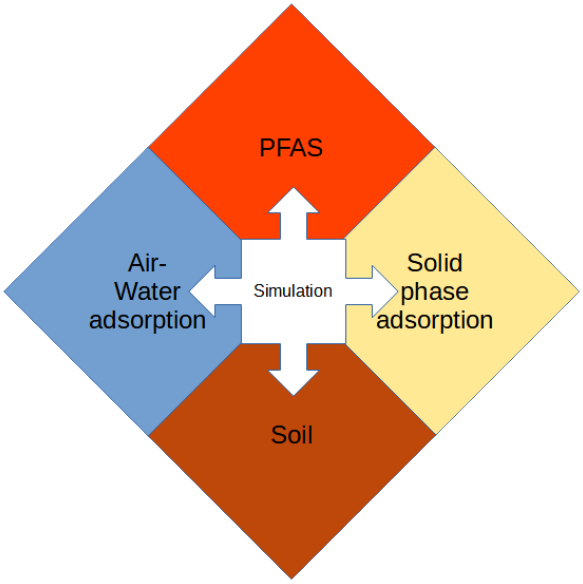

Figure 2.1: Overview of the main modules in the PFAS simulation code. Each PFAS and soil is simulated using a single module, and different sorption models are available for the sorption to AWIs and SWIs. Each module can be interchanged with another module of the same type to simulate different PFASs or different sorption models.

Van Genuchten parameters, as well as the saturated and residual water content, saturated hydraulic conductivity, and ranges for the fractions of organic matter, loam ($d < 50\,\mu m$), and clay ($d < 2\,\mu m$). The Staring series is divided into topsoil and bottom soil classes, which cover the depth ranges of 0 cm to 20 cm and 20 cm to 120 cm, respectively. As the model by Guo et al. (2022) assumes a homogeneous, semi-infinite soil, only the soil classes for the bottom soils where selected. The soil bulk density, ρ_b, is required for calculating the retardation (Equation 1.8). Poelman (1974) established a model for estimating the density of Dutch soils from the soil composition using the following equation:

$$\rho_b = (1-\phi)\left(1.47 \cdot f_{oc} + 2.88 \cdot f_c + 2.66 \cdot (1 - f_{oc} - f_c)\right), \tag{2.1}$$

where ϕ is the porosity, f_{oc} is the fraction of organic carbon, and f_c is the fraction of clay.

The soil water content was determined using the Van Genuchten soil water retention curves, by equating the average groundwater recharge of 300 mm/year to the relative hydraulic conductivity, which is possible because of the unit gradient assumption by Guo et al. (2022), and solving Equations 1.1, 1.2 and 1.3 for θ. Then a beta distribution of the effective saturation was constructed with the mean at the calculated S_w, and a variance of $(0.05 * S_w)^2$, to simulate a small range of values near the expected water content.

The approach for moddeling the adsorption at solid-water interfaces (SWIs) is taken from the paper by Fabregat-Palau et al. (2021), using the measured values when available, and otherwise estimated using the model developed in that study. This uses the fraction of organic carbon in the soil, f_{oc}, and the combined fractions of silt and clay, $f_s + f_c$, to estimate the total partitioning coefficient based on the length of the CF_x chain:

$$K_d = K_{oc} + K_{sc} = 10^{(0.41 \cdot n_{CF_x} - 0.70)} \cdot f_{oc} + 10^{(0.32 \cdot n_{CF_x} - 1.70)} \cdot (f_s + f_c)\,. \quad (2.2)$$

This model assumes no sorption to either sand minerals or metal oxides. The separate values for K_{oc} and K_{sc} also allows the calculation of separate retardation factors for the organic carbon and the soil minerals using Equation 1.8

$$R_s = R_{oc} + R_{sc} \quad (2.3)$$

$$R_{oc} = \frac{\rho_b K_{oc}}{\theta} \quad (2.4)$$

$$R_{sc} = \frac{\rho_b K_{sc}}{\theta} \quad (2.5)$$

Sorption at the air-water interfaces (AWIs) requires estimates for the air-water interfacial area (A_{aw}), and for the partitioning coefficient (K_{aw}). The A_{aw} is estimated using the Leverett thermodynamic model (LTM) (Equation 1.6) as measurements are not available for the soils in the Staring series. To compensate for the underestimation of the surface area, the Surface Roughness Multiplier (SRM), as proposed by Silva et al. (2022), was considered. However, closer inspection of the substantiation of that model learned that it is unable to produce meaningful results (see Appendix C for more information). Lacking data to fit a better model, the only plausible value in the literature, of 4.15 for Vinton soil from Guo et al. (2022), was used for all simulations. The affinity with the AWIs was estimated using the group contribution model by Le et al. (2021). As the model code by Guo et al. (2022) assumes linear sorption, the partitioning coefficient was linearized using the time averaged input concentration, $\overline{C_{aq}}$, as an estimate for the average concentration, resulting in the following equation (derived from Equations 1.5 and 1.7):

$$K_{aw} = \frac{C_{aw}}{A_{aw} C_{aq}} = \Gamma_{max} \cdot \frac{\kappa_{aw}}{1 + \kappa_{aw} \overline{C_{aq}}} \quad (2.6)$$

Dispersion was estimated using the model by Xu and Eckstein (1995):

$$\alpha_L = 0.83(\log_{10} L)^{2.414}, \quad (2.7)$$

where α_L is the longitudinal dispersivity in meter, and L is the characteristic length of the soil in meter. In this study the focus is on the top 1 m of the soil, but as this relationship is only valid for $L > 1\,m$, the characteristic length was fixed at $L = 2\,m$, and therefore $\alpha_L \approx 4.5\,cm$. For many PFASs no diffusivity is available

(Table 2.1), therefore a linear regression was used to estimate the diffusivity based on the number of CF_x groups in the molecule:

$$D_0 = 10^{(-4.536-0.1088\cdot n_{CF_x})}. \tag{2.8}$$

For each column 300 simulations were run with random combinations of f_{oc}, f_s, f_c, and the jittered θ values, as well as a simulation with the mean parameterization for that soil class. For each simulation the variable input parameters were recorded, as well as intermediate results, such as A_{aw}, K_d, K_{aw}, and the retardation factor, R. Also, the concentration of the PFAS over time at a depth of $z = 1\,\mathrm{m}$, and the total mass of PFAS adsorbed to AWIs and SWIs in the interval $0\,\mathrm{m} \leqslant z \leqslant 1\,\mathrm{m}$ were recorded as a function of time.

Chapter 3

Results

3.1 Model parameters

The Staring series soils are classified by the fractions of silt, clay, and organic carbon (Figure 3.1), and in case of the sandy soils also by the grain size distribution. The sandy soils O01 to O04 are characterized by fine sands (median grain sizes, M_{50}: 105 µm to 210 µm), increasing amounts of silt, no clay, and at most 3 % organic carbon. Soil O05 represents coarse sand (M_{50}: 210 µm to 2000 µm) with no silt or clay. Soil O06 is boulder clay with up to 50 % silt and a wide range of sand particle sizes (M_{50}: 50 µm to 2000 µm), and soil O07 is brook clay that contains 33 % to 50 % silt and very fine sand particles (M_{50}: 50 µm to 150 µm).

The loamy and clayey soils contain no silt, but an increasing fraction of clay (Figure 3.1b), from 8 % to 12 % in loamy sand (O08) to 50 % to 100 % in clay (O13), and at most 3 % organic carbon. The silt soils (O14 and O15) contain a large amount of silt (Figure 3.1a), but no clay and at most 3 % organic carbon. Finally, the peat soils contain no silt or clay, but a large fraction of organic carbon, up to 100 % (Figure 3.1c). Peaty sand (O18) is a special case of the peaty soils, containing both a large fraction of sand, and a large fraction of organic carbon.

In order to determine the available air-water interfacial area (A_{aw}) in the soil it is first necessary to determine the effective soil saturation at the given recharge rate. Sandy soils are typically the least saturated at $q = 300$ mm/year (see Figure 3.2a), with the coarse sand (O05) saturated at 20 % to 27 % of the maximum water saturation. The loamy soils (O08 – O10) show a transition to higher saturations, towards clayey soils that are nearly fully water saturated to sustain the same discharge. The silt soils (O14 and O15) show a similar trend, with the O14 soil being less saturated, more alike the sandy soils, while the O15 soil is more saturated, more alike the loamy soils, which correlates with silt content of these two soils (Figure 3.1a). Finally, the peat soils O16 and O17 are similarly saturated at this recharge rate due to similar composition and Van Genuchten parameters, while the peat soil O18 contains more sand, and is therefore less saturated.

The A_{aw} is then calculated from the water saturation using the LTM. In the sandy soils $A_{aw} \approx 500$ cm²/cm³ (Figure 3.2b), which is the result of the relatively low

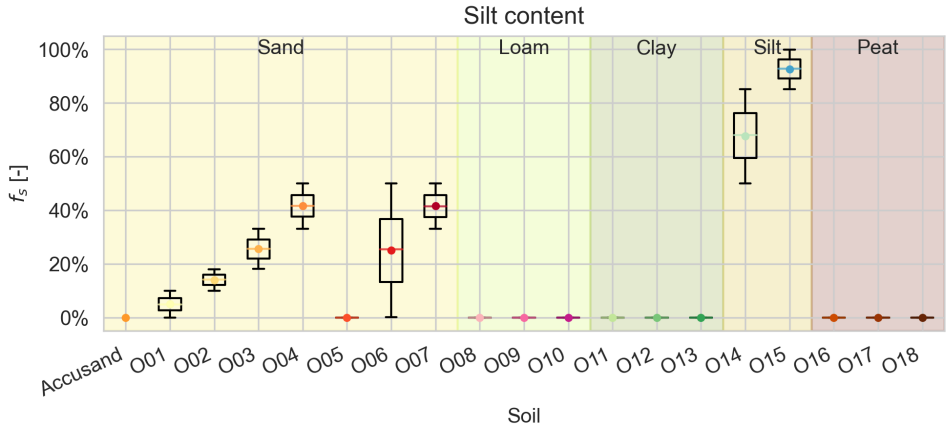

(a) Silt content, f_s

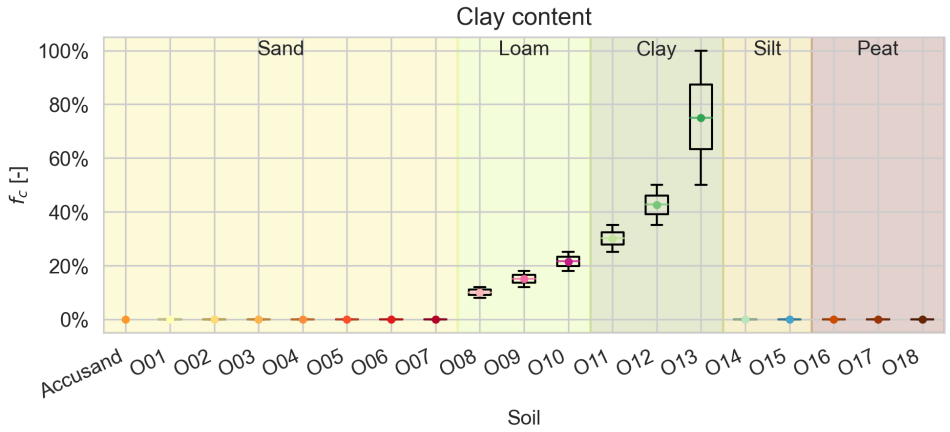

(b) Clay content, f_c

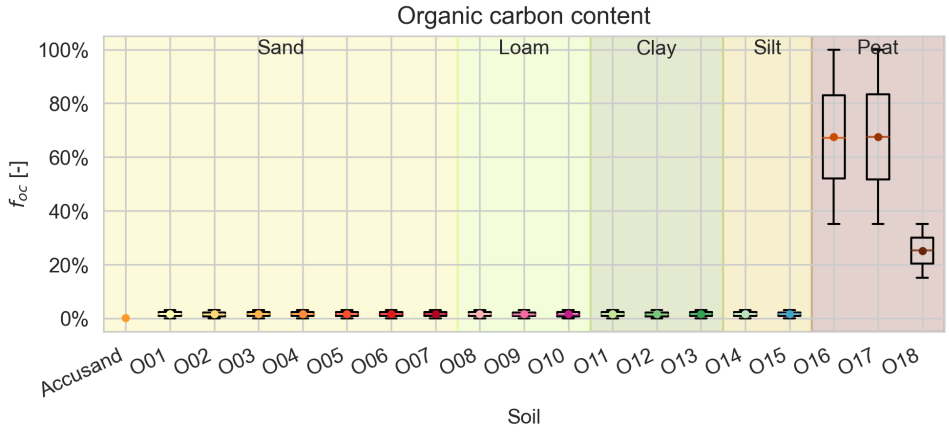

(c) Organic carbon content, f_{oc}

Figure 3.1: Soil composition of the Staring soils.

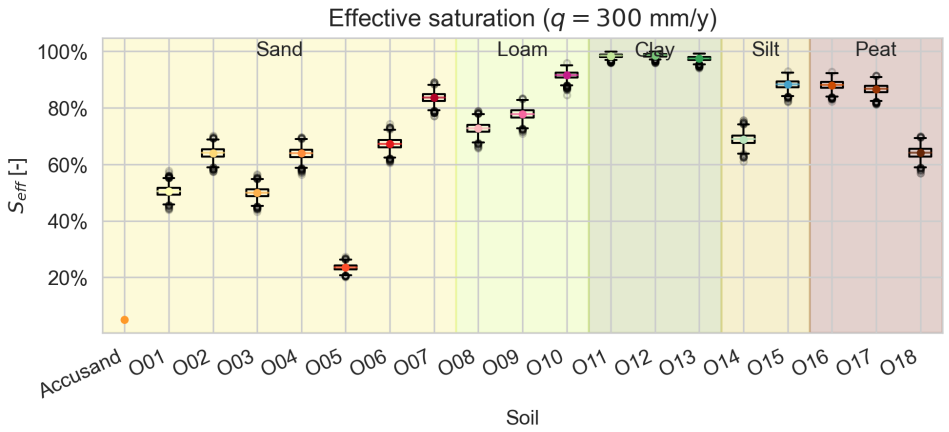

(a) Distribution of the effective saturation for the different soil types. The dark dots above and below the whiskers indicate extreme values, which are caused by the jittered values for θ. For Accusand no distribution is available on the distributions of the soil properties and therefore only the mean effective saturation is shown.

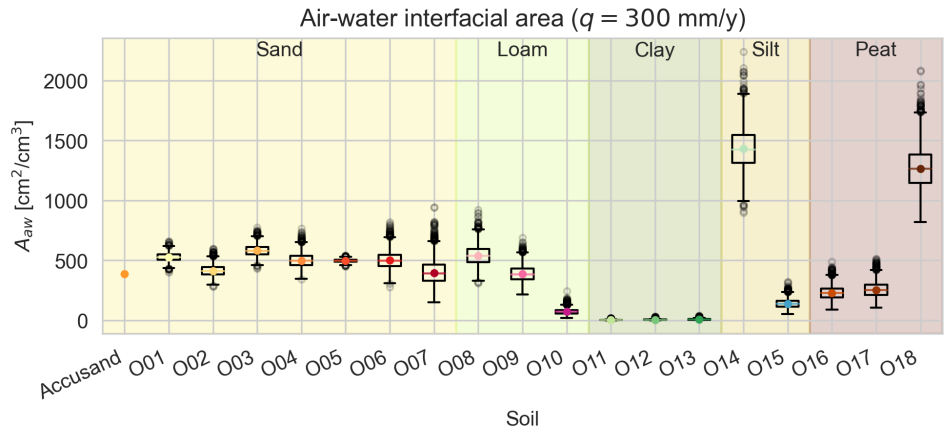

(b) Distribution of the air-water interfacial area for the different Staring soil types. The dark dots above and below the whiskers indicate extreme values.

Figure 3.2: Effective saturation and air-water interfacial area of the Staring soils.

effective water saturation. For soil O05, the A_{aw} shows a very narrow distribution, which is means this soil type is insensitive to changes in the effective water saturation in the range of saturations considered. The loamy soils have a similar A_{aw} to the sandy soils, with a transition to the clayey soils, for which $A_{aw} \approx 0$ cm^2/cm^3, as these soils are close to their maximum water saturation. The silty soil O14 has a large spread in the estimated A_{aw}, in the range of 1000 cm^2/cm^3 to 1800 cm^2/cm^3, while soil O15 has a much smaller A_{aw} at approximately 50 cm^2/cm^3 to 250 cm^2/cm^3. The peaty soils O16 and O17 have a slightly smaller A_{aw} than the sandy soils, around 250 cm^2/cm^3, while the peat soil O18 has a similar A_{aw} to the silty soil O14.

The affinity of PFASs with the AWIs is different for each PFAS, and is parameterized in the partitioning coefficient K_{aw}. The partitioning coefficients are calculated using the PFAS properties, such as the length of the CF_x tail, and the type of active head. TFA shows the least affinity with AWIs, meaning its tail is less hydrophobic compared to the hydrophilicity of its head (Figure 3.3a). For longer PFASs, the partitioning coefficient increases, meaning the hydrophobicity of the tail increases up to PFDA, which has the largest affinity with the AWIs of the PFASs considered. The sulfonic acids have a larger affinity with the AWIs than the carbonic acids with the same number of carbon atoms (compare perfluorobutane sulfonic acid (PFBS) and perfluorobutanoic acid (PFBA)), because in the sulfonic acids all carbon atoms are fluorized, while in the carbonic acids the last carbon atom is part of the carbonic acid head. An outlier from this trend is HFPO-DA, which has 5 CF_x groups, but a shorter effective chain length because it is a dimer of two shorter chains.

The partitioning coefficient for sorption to the solid phase, K_d, depends on the soil composition, as well as the type of PFAS under consideration (Equation 2.2). When aggregated per soil, the values for K_d span multiple orders of magnitude (Figure 3.3b), with the smallest values in Coarse sand (O05), which contains no fine particles, and very little organic matter. The largest K_d values are observed in peat soils O16 and O17, as these soils consist almost entirely of organic matter, and the K_{oc} of most PFASs is one or two orders of magnitude larger than the K_{sc} (Table 2.1).

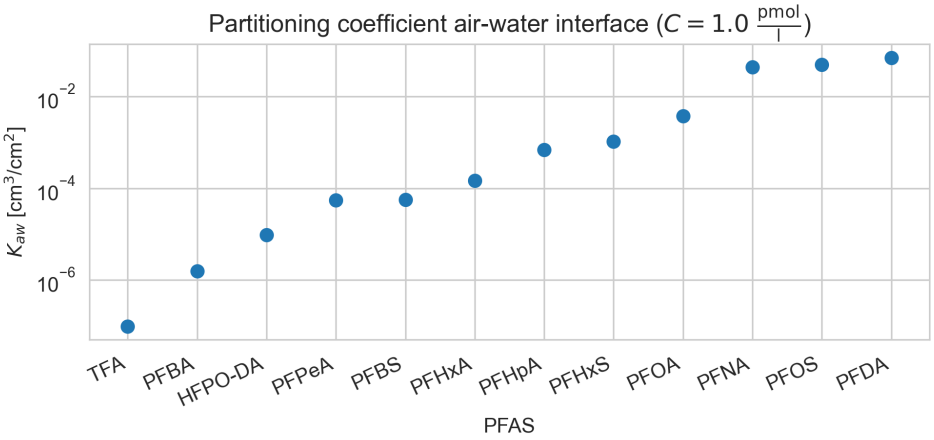

(a) Distribution of the air-water partitioning coefficients for the considered PFASs.

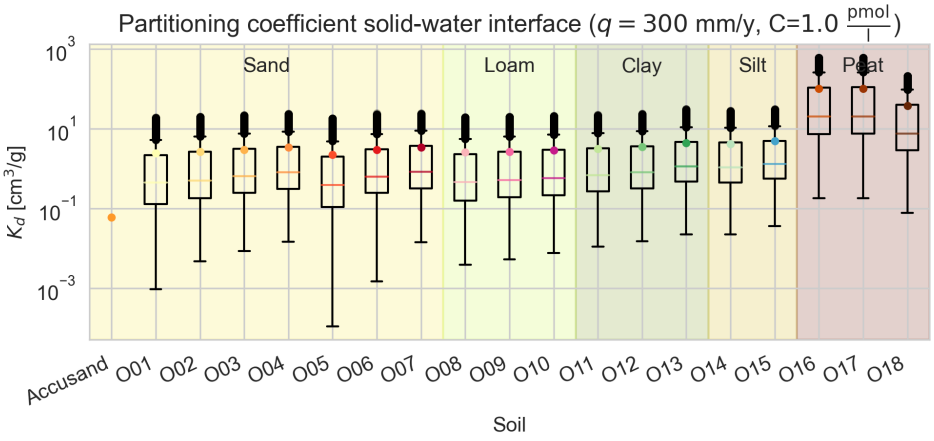

(b) Distribution of the solid-water partitioning coefficients for the Staring soils.

Figure 3.3: Partitioning coefficients from the water phase to AWIs and SWIs.

3.2 Retardation

The retardation factor calculated from Equation 1.8 shows that long chains, such as perfluorooctane sulfonic acid (PFOS) and PFDA are retarded more than shorter chained PFAS compounds, such as TFA and PFBA (Figure 3.4). For example, when looking at the soil type O05, the retardation factor of TFA (with a tail length of 1) is approximately 1.15 and of PFBA (tail length of 3) is 1.87, while PFASs with a tail length of 8, PFOS and PFNA, have a retardation factor of 471 and 344, respectively.

Similarly, PFASs with sulfonic acid as the active group show more retardation than those with the same carbon chain length but carbonic acid as the active group, compare for example PFBA and PFBS, or PFOA and PFOS. As mentioned before regarding the air-water partitioning coefficient, K_{aw}, this is because in case of the carbonic acid one carbon atom is part of the COOH group, and not part of the hydrophobic CF_x tail. For short tailed PFASs this most notably affects the R_{oc}, with values of 0.86 and 3.44 for PFBA and PFBS on sandy soil O05, respectively, although the R_{aw} increases from 8.9×10^{-3} to 0.32 for the same PFASs. For longer tailed PFASs the difference in R_{oc} and R_{aw} is more similar, again comparing in Staring soil O05, PFOA and PFOS have an R_{oc} 32.4 and 189, respectively, and an R_{aw} of 21.7 and 281.

As the soils in Figure 3.4 are sorted by the total retardation of PFOA, a number of patterns can be observed in the retardation in different types of soils. For example, the clay soils have the least retardation for all different PFASs, and virtually no retardation by air-water interfaces, with the R_{aw} of PFDA in clay soil O12 being 0.50, or 3 % of the total retardation in that soil. The loamy soils show a similar amount of retardation as the clay soils for the shorter PFASs, but because the A_{aw} is larger in the loamy soils, the retardation by air-water interfaces is larger than in the clay soils for longer tailed PFASs.

Based on the spread of the retardation factors, TFA, perfluorohexanoic acid (PFHxA), PFOA and PFDA were selected for further analysis with respect to different PFAS, while soil classes O05 (sand), O12 (clay), O15 (silt) and O18 (peat) were selected for the comparison of different soils in order to get a balanced distribution of different soil classes.

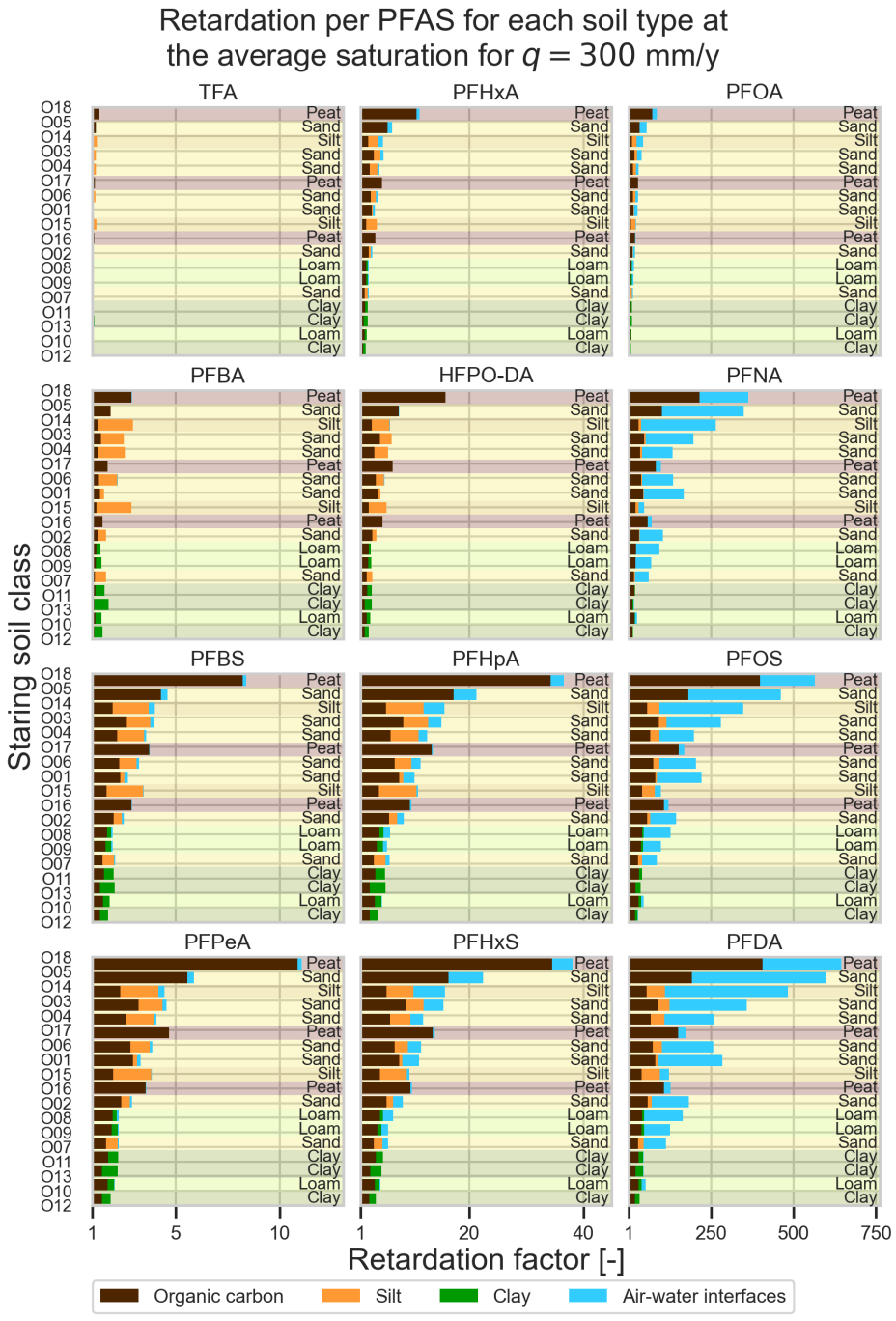

Figure 3.4: Mean retardation factors for all combinations of PFASs and Staring soils. Each bar shows the retardation factor in a soil, with colours representing the cause of retardation. The plots for the different PFASs are sorted in columns by the mean retardation of that PFAS (note the different horizontal scales for each column), and the soils within the plot are sorted by the mean retardation for PFOA. The colours of the background represent the soil class, labelled on the right.

3.3 Breakthrough curves

The breakthrough curves of TFA show that the peak concentration is reached faster in sandy soils than in clay soils (Figure 3.5), with the retardation in the clayey and peaty soils entirely caused by sorption to solids. There is no noticeable sorption of TFA to the AWIs in any of the soils. This also results in the time to breakthrough at $z = 1\,\mathrm{m}$ for TFA to be determined by the water velocity in the soil.

For PFHxA the curves show a similar pattern, albeit with a slight amount of sorption to AWIs, and more adsorption to solid-water interfaces. Most notably, the breakthrough curve for PFHxA in the peat soil (O18) is retarded significantly, with the peak concentration only reached after approximately 30 year, which is caused by sorption to SWIs. In the other soils the SWIs and AWIs are saturated within 10 year, which can be seen as a horizontal line in the accumulation on SWIs.

For PFOA, retardation starts to affect the breakthrough in all soils considered, with the Sandy clay (O12) leaching marginally faster than the coarse sand (O05). The Sandy peat (O18) shows the most retardation due to sorption to both solids and AWIs. Initially all PFOA in soil O18 is adsorbed to either the SWI or AWI, which is visible in the linear increase in the accumulation, and the sum of the accumulation on SWI and AWI at $t = 25\,\mathrm{year}$ being 1.

Finally, for PFDA, the adsorption in the Sandy peat (O18) is so strong that virtually no PFDA leaches within 250 year after the contamination input period starts. Leaching of PFDA from the Silt loam (O15) and Coarse sand (O05) is approximately equally fast. However, in the loamy soil this is almost entirely due to sorption to solids, while in the coarse sand this is largely due to the adsorption to AWIs, which means the patterns in the breakthrough curves alone cannot give information on the processes behind the retardation.

The breakthrough curves determined with multiple realizations of the soil composition from the Staring series distributions show that for the larger retardation factors the bandwidth of potential breakthrough curves increases (Figure 3.6). Note that Accusand is missing from this comparison because it is a synthetic soil with a fixed composition.

In the peaty sand (O18) the breakthrough curves show the largest bandwidths compared to the other soils, although for PFDA there is no leaching in any of the simulations. In the coarse sand (O05) the bandwidths are smaller, but for PFOA it shows that in a large fraction of the simulations the peak is reached within the 25 year contamination input period, even though the mean parameterization predicts the peak is reached after 30 year. The silt loam (O15) shows similar behaviour to the coarse sand, although in this case all PFOA simulations show the peak later than 25 year. The clayey sand (O12) shows the smallest bandwidths in the time to peak concentration in the breakthrough curves for all PFASs considered. However, the bandwidth in the peak concentration itself is largest for PFDA in soil O12, showing a range between 0.4 pmol/L to 0.8 pmol/L.

The bandwidth in the times to peak concentration, and the bandwidth in the

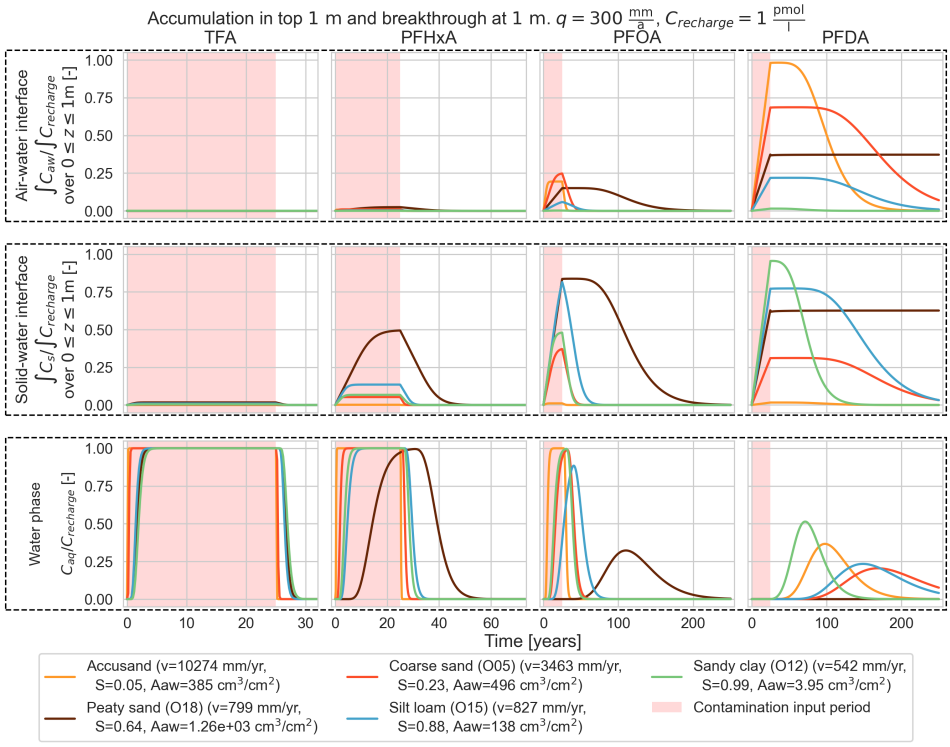

Figure 3.5: Accumulation of PFAS in the top 1 m of the soil over time, of which adsorbed to air-water interfaces (top row), and to solid-water interfaces (middle row), and breakthrough curves at a depth of $z = 1$ m (bottom row).

peak concentrations themselves is visualized in Figure 3.7. The distributions are centred around the peak of the reference simulation with the mean parameters (orange lines in Figure 3.6), and cover the 95 % Highest Probability Density Interval (HPDI) of the distribution.

For TFA the adsorption sites are saturated within 25 year for all simulations, which is visible in the height of the HPDI in the peak concentration being 0 pmol/L. The contamination reaches a depth of 1 m at first in sandy soils, then silt, clay, loam, and finally peat soils. Peaty sand (O18) leaches faster than the other peat soils (O16 – O17), because the hydraulic conductivity of the peaty sand is higher, and as discussed before, TFA shows very little sorption to any of the soils. The largest bandwidth in the time to peak is seen in the peaty soils, in the order of 3 year, while the smallest bandwidths are in the sandy soils, of approximately 1 year.

For PFHxA the pattern is the same, although in peat soils the retardation is sufficient to lower the peak concentration below 1 pmol/L. Also, the transport in the loamy and peaty soils is retarded enough to increase the time to peak concentration until after the 25 year contamination input period.

In the simulations of PFOA transport the peak concentration is not reached

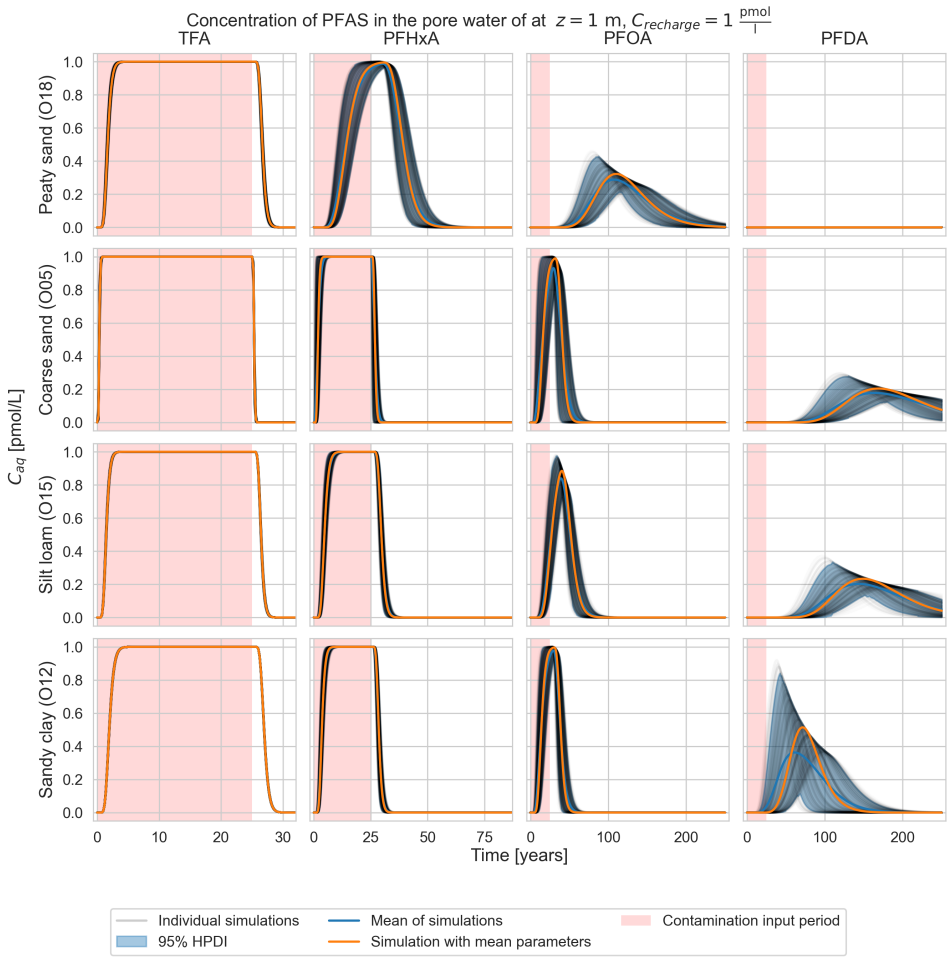

Figure 3.6: Bandwidth in breakthrough curves from multiple simulations with varying soil composition and water content. Note that Accusand is not included as it is a synthetic soil with a fixed composition.

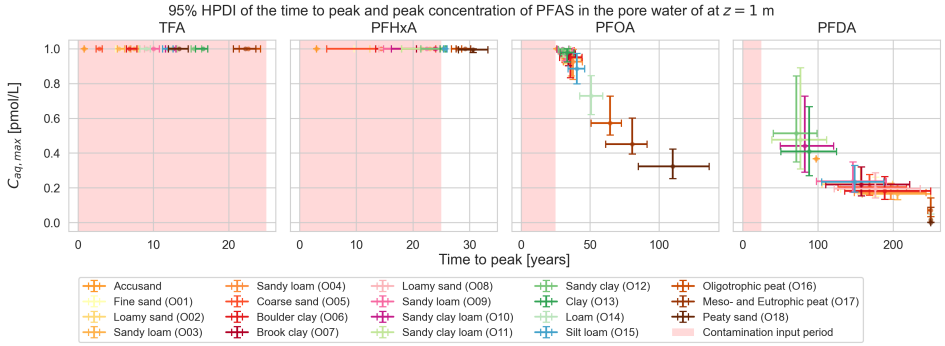

Figure 3.7: Distribution of time to peak concentration and peak concentration of four PFASs in all soils from the Staring series

within the 25 year contamination period for any of the Staring soils, but for most soils before 50 year. Notable exceptions are the peat soils (O16 – O18) and Loam (O14), with the peaty sand (O18) stretching up to 130 year to reach the peak concentration.

With PFDA the leaching behaviour is clearly separated in 3 clusters. First of all the clayey soils O10 – O13 arrive within a 50 year to 130 year period. After that the sandy and loamy soils, as well as the silt loam (O15), arrive in the window of 90 year to 250 year. Finally, the peaty soils and loam (O14) arrive later than approximately 240 year, although the peaty sand (O18) never peaks within 250 year.

Chapter 4

Discussion

4.1 Sorption to air-water interfaces

4.1.1 Interfacial area

The total amount of sorption to air-water interfaces (AWIs) depends directly on the amount of air-water interfacial area (A_{aw}) available, but at the same time there are no validated measurements of these values in Dutch soils. Therefore, the values for A_{aw} are estimated using the Leverett thermodynamic model (LTM) multiplied by a roughness multiplier (SRM). The SRM used in this study is purely based on the reported value of 4.15 in Guo et al. (2022), and in that case the value is the average over different measurements on a specific soil at different saturation levels. From Equation 1.5 and Equation 1.8 it follows that the contribution of the SRM to the total retardation is linear. In cases such as the retardation of PFDA in Staring soil O05, the current model predicts 70.9 % of the total retardation to be due to sorption to AWIs. However, if the multiplier is reduced by a factor of 0.5 to 2.075, the contribution of the air-water sorption is reduced to 55.0 %.

4.1.2 Water saturation

This study only considered a recharge rate of 300 mm/year, which is the average recharge rate in the Netherlands. At lower recharge rates, and thus lower saturation, several Dutch soils show a large increase in A_{aw} according to the LTM (Figure 4.1), much larger than Accusand. The Coarse sand (O05) shows the most similar trend to Accusand, but the other Staring soils show a much larger increase in A_{aw} towards lower recharge rates. This is caused by the larger porosity of the Staring soils combined with finer soil textures, which results in a larger maximum A_{aw}. This is consistent with the findings of (Silva et al., 2022), who argued that the A_{aw} in finer textured soils is larger than in coarser soils, but also that the SRM increases for finer soils and broader distributions of particle sizes. That would mean that the differences in the A_{aw} between the Staring soils is even larger than what is shown in Figure 4.1.

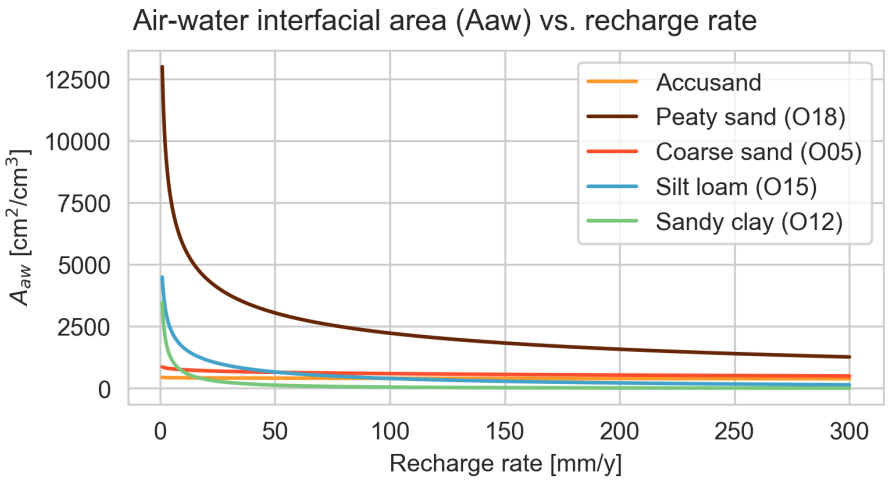

Figure 4.1: Comparison of the A_{aw} for the selected Staring soils at different recharge rates (SRM = 4.15). Note that at the same recharge rate the saturation is different for the different soils (see also Figure 3.2).

To improve the estimates a better model for the A_{aw} is therefore required, that takes into account the roughness of the soil particles. This is especially important at low water saturation where the water film follows the surfaces of the soil particles (Jiang et al., 2020; Silva et al., 2022), and thus in the sandy soils that are on average less saturated than finer grained soils. Silva et al. (2022) proposed a model to estimate the roughness multiplier, but that paper was found to be not reproducible (see also Appendix C). The authors claim the relationship between the Soil Surface Roughness Factor (SRF) and the Surface Fractal Dimension (D_s) is linear, but do not report the correlation coefficient, which turns out to be close to 0. They then claim to use that slope for extrapolation of the relationship between the SRM and SRF, but the equation they report cannot reproduce the values presented in the paper, nor does it show how the slope from the SRF-D_s relationship is incorporated. However, the idea of using the D_s to estimate the SRM as hinted on by Silva et al. (2022) is interesting, as there is a relationship between the Van Genuchten parameters and the D_s (Ghanbarian et al., 2021). If a proper relationship between the SRM and the D_s and water saturation is found, the SRM could be estimated from the Van Genuchten parameters directly when no measurements of the A_{aw} are available. In order to construct such a model, more measurements in different soils and under varying soil moisture conditions are required.

4.1.3 Temporal emission profiles

Over the past decade PFOS and PFOA have been prohibited from use in industrial applications, and they are now being replaced by the shorter chained PFASs PFBS

and HFPO-DA, respectively (U.S. EPA, 2022a; U.S. EPA, 2022b). For the PFASs shorter than PFOA (tail length of 7 CF_x) the effect of AWI sorption is less important than for the longer chains (Figure 3.4). Therefore, even though PFOA and PFOS were deposited further in the past, their replacements will experience less retardation, and thus reach the groundwater faster. Compounds that have been deposited sequentially might therefore reach the groundwater in a different order. In order to provide more accurate predictions of future PFAS concentrations in the groundwater, it is therefore important to gather more information on historical and current deposition rates of PFASs, as well as on the source locations of these contaminations.

4.2 Sorption to solid-water interfaces

4.2.1 Sorption mechanisms

The model for the partitioning of PFAS to solid-water interfaces (SWIs) is based on the amount of organic matter and fine mineral fraction. However, no distinction is made between different causes for adsorption. Adsorption could take place by electrostatic sorption, in which the ionic head of the molecule attaches to the soil particles and the tail directed towards the pore water. Alternatively, the hydrophobic tail could sorb to the soil particles, with the ionic head directed into the water, similar to the sorption at AWIs (Jiang et al., 2020). From field studies it is known that several PFASs can be effectively removed from solution using Ion Exchange reactors, which rely on electrostatic sorption (Pannu & Plumlee, 2021). For these reactors, adsorption is more or less irreversible unless a concentrated electrolytic solution is used for regeneration. If irreversible sorption to solids is present in natural soils, the current model overestimates the leaching, or underestimates retardation to the solid phase, specifically for soils with relatively high silt or clay contents. Batch experiments with different soil minerals and PFASs are required to determine which sorption processes are dominant on natural soils, and to what extent the adsorption is reversible.

4.2.2 Branched PFASs

The model by Fabregat-Palau et al. (2021) estimates the partitioning coefficient for the organic carbon and mineral fractions purely based on the number of CF_x groups in the PFAS molecule. However, in the model by Le et al. (2021) for the sorption to AWIs a larger number of features of the molecule is taken into account, which appears to be especially important for branched PFASs, such as HFPO-DA. From the K_{aw} for HFPO-DA compared to the unbranched PFASs in Figure 3.3a it appears that either the hydrophobicity of the tail of these molecules is lower compared to its hydrophilic head than in a PFHxA molecule, an unbranched PFAS with the same number of CF_x groups, or the surface area occupied by a molecule of

HFPO-DA on the interface is larger, resulting in a lower Γ_{max} (Rosen, 2004). In both cases it would mean that HFPO-DA would be even more mobile than currently estimated.

4.2.3 Peat soils

Sorption to peaty soils is estimated to be relatively large compared to sandy soils due to the carbon content of up to 100 %. It is unlikely that the results presented in this study are representative of the PFAS leaching in such soils. Apart from the high organic carbon content, the unsaturated zone in these soils is kept artificially as small as possible to prevent peat from oxidizing and causing land subsidence (Querner et al., 2012), thus leading to a higher water saturation and smaller a A_{aw}. Moreover, peat soils tend to swell and shrink with changes in water saturation (Camporese et al., 2006), and thus the assumption in the calculation of the partitioning coefficient that the interfacial area is constant is invalid (see also Appendix B).

4.2.4 Saturated zone

Sorption to SWIs is not only relevant in the unsaturated zone, but also in the saturated zone. As the PFAS compounds are transported towards the groundwater, the water saturation of the soil increases, and thus the A_{aw} decreases. This means that sorption to SWIs gains in importance compared to AWIs, and in the saturated zone the PFAS compounds are only retarded by sorption to SWIs. Therefore, improved understanding of the sorption of PFASs to the solid phase will improve models of PFAS transport in the saturated zone as well.

In the case of drinking water supply a large part of the residence time in the subsurface is spent in the saturated zone. Thus, even though adsorption to AWIs is the dominant retardation mechanism in the unsaturated zone for longer PFASs, and affects the time it takes for the compounds to reach the groundwater, it is the sorption to SWIs that determines the concentrations in the extraction wells for drinking water supply.

4.3 Steady state modelling

The retardation of PFAS compounds by sorption to AWIs depends on the saturation (Figure 4.1), and it is thus to be expected that transport of PFAS compounds is non-linear with variations in the recharge flux. The screening model used in this study assumes steady state flow, and therefore does not take into account the effect of variable saturation on the sorption. During peaks in precipitation soils can become temporarily saturated, which removes the sorption to AWIs entirely. On the other hand, during drier periods the A_{aw} increases (Figure 4.1) and pore water can become stagnant, which will increase the retardation.

According to KNMI (2023b), on 73 % of the days the precipitation in De Bilt, The Netherlands, is less than the daily mean precipitation, which suggests that the effect of sorption to AWIs could be larger than currently estimated. Due to the higher porosity of clay soils, the maximum A_{aw} is higher for clay soils than for sand soils (Figure 4.1). This is amplified by the potential of clay soils to form cracks when drying (Vogel et al., 2005), which is not included in the LTM. This also means that under very dry conditions the effect of sorption to AWIs in clay soils is larger than in sand soils, but at the same time preferential flow paths could lead to faster leaching. At the same time, peaks in precipitation on clay soils can lead to overland flow and thus reduce the actual recharge.

At this point it is not clear whether temporary saturation or prolonged drier periods have a stronger effect on the average leaching rate of PFAS compounds in the unsaturated zone, especially when combined with heterogeneities in the soil (see also section 4.4). Also, hysteresis causes different water saturation levels during drainage and imbibition, which according to Chen et al. (2007) should be modelled by including the A_{aw} itself in the calculation of the soil water retention curves. To investigate this, it is recommended to construct 2D models of the unsaturated zone that include the effect of variable precipitation. It is also necessary to perform column experiments with different soil types under varying soil moisture conditions for validation of the model results.

4.4 Natural soils

The analytical solution employed in this study assumes a semi-infinite unsaturated zone of a single soil type. However, natural soils in the Netherlands are stratified into layers, with the Staring series representing building blocks for these individual layers to build up a representation of a natural soil (Heinen et al., 2020). When these materials are stacked, especially under transient flow conditions, the transition between these materials can strongly affect the hydraulic conditions, with perched water due to differences in the soil water retention curves, and thus affect the transport of PFASs.

Clay soils can have very low hydraulic conductivity, yet in the Staring series the lowest hydraulic conductivity is estimated at 1.08 cm/d or 3.94×10^3 mm/year for the Sandy clay (O12). One possible explanation is that the saturated hydraulic conductivity in Heinen et al. (2020) is fitted on the geometric average of multiple soil water retention curves and the corresponding unsaturated hydraulic conductivity curves, and thus extrapolated from the data. As a consequence, these soils might in reality not be able to sustain a continuous discharge of 300 mm/year. The saturation of these soils is most likely close to saturation, as modelled in this study, but the actual flow velocity would be lower than predicted. This means that it is plausible that leaching from clayey soils is not faster than from sandy soils, but further research is required.

Coastal dunes are an important source of drinking water in the Western parts of the Netherlands. However, the well sorted sands in these dunes are not well represented by any of the building blocks in the Staring series (Verburg, 1995). PFAS compounds are found to be enriched in sea spray aerosols, which are then deposited on the dunes (Sha et al., 2021). At this point there is insufficient data to assess the leaching behaviour in these dunes, and therefore further research into both the transport of water, and that of PFASs in coastal dunes is required.

Finally, Rosen (2004) states that the partitioning of PFAS compounds between the water phase and AWIs is likely to increase with decreasing temperature, although no model exists to estimate the magnitude of that increase. This is because at lower temperatures the thermal motion of PFASs is reduced, which reduces the surface area occupied by a single molecule at the interface, thus increasing the number of sorption sites. As most measurements of the K_{aw} of PFASs are performed at room temperature, in the range of 20 °C to 25 °C, and the average soil temperature in De Bilt is 11.1 °C (KNMI, 2023a), the K_{aw} values in this research are possibly underestimated. To ensure that future laboratory measurements of the sorption characteristics of PFASs are representative of the field conditions, it is recommended to perform these measurements at a lower temperature, or at the very minimum assess the differences in these characteristics at different temperatures.

4.5 Comparison to measurements

Data from Wintersen et al. (2021) suggests that PFOA leaches faster than estimated in this study, with concentrations up to 10 ng/L or 24 pmol/L at a depth of 25 m. Results from this study suggests PFOA is transported at most $\frac{1}{25}$ m/year (Figure 3.7), so it would take at least 625 year to reach that depth while PFOA was only produced since 1949 (Paul et al., 2008). This is likely due to a combination of factors, including a stronger vertical gradient in the piezometric head which increases the advection, but also a higher water content towards the groundwater fringe due to capillary effects, whereby the retardation by AWIs decreases with depth. Furthermore, heterogeneities can cause preferential flow paths, which in turn can speed up PFAS transport, although depending on the scale of the model compared to the scale of these preferential flow paths, the latter are partially captured in the dispersivity of the soil. Therefore, even under steady state flow conditions, the PFAS advection will increase.

In another study, the Dutch national railways (NS) investigated the concentration of PFASs in the soils on their properties potentially influenced by atmospheric deposition from nearby waste processing plants (Verschragen, 2019). Samples were taken at approximately 0 cm to 20 cm and 20 cm to 50 cm depth, and analysed for PFAS concentrations. In these measurements mainly PFBA, PFOA and PFOS were found.

The measurements show that in one location the concentrations of PFOA and PFOS are higher in the deeper samples than in the shallower samples (location B in Table 4.1), while the concentration of the shorter chained PFBA was found to be higher in the shallower samples. If we assume that the hydraulic parameters are the same for all PFASs, and that the PFASs were introduced at the same time, this would suggest that the shorter chained PFASs are transported slower than the longer chained PFASs. However, even if the absolute values of the retardation factors for the different compounds as estimated in this research are not correct, it is unlikely that the retardation of PFBA is higher than that of PFOA or PFOS (Fabregat-Palau et al., 2021; Le et al., 2021). It is therefore likely that the shorter chained PFASs were introduced at a later time, which is also consistent with the observation that PFOA and PFOS, once prohibited, were replaced with shorter chained alternatives (U.S. EPA, 2022a; U.S. EPA, 2022b).

Location Od in Table 4.1 shows higher concentrations of all three PFASs in the shallower samples than in the deeper samples, as well as different ratios between the PFASs, showing that the composition of the groundwater recharge varies not only in time but also in space. It should be noted that all these values are based on a single sampling, and therefore do not provide information on the temporal variability at these locations, or the reproducibility of the measurements. This further obviates the need for investigation of historical deposition profiles in different regions of the Netherlands.

Table 4.1 also shows that the measured f_{oc} is higher than for the bottom soils in the Staring series (Figure 3.1), which contain up to 3 % organic carbon, and more like the topsoils of the Staring series, which contain up to 15 % organic carbon (Heinen et al., 2020). This does conflict with the assumption in the Staring series that the high values of f_{oc} only occur in the top 20 cm of the soil, but this could also be caused by the fact that in built-up areas most of the soils are altered by human activities. At these high organic carbon contents the retardation of PFASs is expected to be stronger than what is used in the current research. The data for location Od also shows that the f_{oc} can vary over small depth intervals, with the

Table 4.1: Comparison of the measured concentrations of PFASs at two of the NS locations. The concentrations of PFOA and PFOS are the sum of branched and linear isomers.

Location code	Depth / cm	PFBA / $\mu g/kg_{ds}$	PFOA / $\mu g/kg_{ds}$	PFOS / $\mu g/kg_{ds}$	f_{oc} / %
B	0–20	0.13	0.25	0.38	5.0
B	20–50	0.11	0.35	0.56	5.0
Od	0–20	0.30	1.3	0.72	5.2
Od	20–50	0.12	0.59	0.59	2.5

f_{oc} at 20 cm to 50 cm being less than half of the value at 0 cm to 20 cm.

In a future study, by combining the depth profiles of the PFASs concentrations for each location, and assuming the same hydraulic parameters for each profile, some more information can be obtained about the historical input of the different PFASs. This does require that sufficient data is available on the sorption characteristics of the PFASs in the soil at that location.

Chapter 5

Conclusion

The numerical experiments of the leaching behaviour of PFASs in Dutch sandy soils show many similarities with the results from previous work on American soils. In general, it can be concluded that the shorter the PFAS molecule, the faster it will leach from the soil, due to less sorption to both the AWIs and SWIs. Also, the leaching of long chained PFAS compounds (longer than PFOA, tail length of 7) from clay soils is expected to be faster than from the sandy soils, due to the high water saturation of the clay and resulting small A_{aw}. The leaching from soils with high organic carbon contents, such as peaty soils, is expected to be slowest, due to the large partitioning coefficients associated with the sorption of PFASs to organic matter.

The sorption of PFAS compounds to the AWI was found to be a significant factor in the retardation of PFASs with a tail length longer than that of PFOA in the unsaturated zone, especially in the sandy and loamy soils. The exact amount of retardation depends on the A_{aw} in the soil, but measurements in Dutch soils are not available. The LTM provides a method to estimate the A_{aw} from soil water retention curves, but depending on the soil composition the estimated A_{aw} deviates significantly from measurements, and therefore needs an additional Surface Roughness Multiplier (SRM), to correct this. Currently, no model exists that can be used to estimate the A_{aw} in Dutch soils. It is therefore recommended to gather data on the A_{aw} in the Dutch soils, and to use this data to try to develop a model for the relationship between the soil moisture retention curves and A_{aw}.

Because the Dutch soils are richer in organic matter on average, leaching is expected to be slower than from their American counterparts. However, current models for the sorption of PFAS compounds to the SWI do not take into account the complex molecular structure of the PFASs, or different sorption processes on natural soils, such as the sorption to metal oxides together with significant amounts of organic matter. Measurements of the sorption of PFASs to the different minerals and organic matter in Dutch soils are required to develop more complete models for the sorption to SWIs. This would also improve the understanding of the sorption, and thus transport, of PFASs in the saturated zone.

In this research the transport of PFAS compounds is modelled in steady state,

but since soil water retention curves are non-linear and as a result the A_{aw} is non-linear as well, it is unclear whether the results are representative for the actual transport in the unsaturated zone. Also, the model does not take into account the effect of layers of different soil materials, which is expected to have a significant effect on the transport of PFASs in natural soils. A first step to improve on this would be to use a 2D model to simulate variations in precipitation and the resulting variations in the soil moisture conditions, which should also be validated using column experiments.

Currently, no data is available to validate the results of this study directly. However, data from other studies suggest that the leaching of PFAS compounds to the groundwater can be significantly faster than what is estimated from this study. In order to validate the results of this study, it is recommended to perform column experiments with Dutch soils, but in order to improve estimated future concentrations in the groundwater, it is also necessary to gather data on the historical deposition rates of PFASs in the Netherlands.

Bibliography

Aa, N. van der, Hartmann, J., & Smit, C. (2022). PFAS in Nederlands drinkwater vergeleken met de nieuwe Europese drinkwaterrichtlijn en relatie met gezondheidskundige grenswaarde van EFSA. https://doi.org/10.21945/RIVM-2022-0149 (cited on page 1).

Alfaro Garcia, L. A., Descamps, S., Herzke, D., Chastel, O., Carravieri, A., Cherel, Y., Labadie, P., Budzinski, H., Munoz, G., Bustamante, P., Polder, A., Gabrielsen, G. W., Bustnes, J. O., & Borgå, K. (2022). Bioaccumulation of per and polyfluoroalkyl substances in Antarctic breeding south polar skuas (Catharacta maccormicki) and their prey. *Frontiers in Marine Science*, *9*. https://doi.org/10.3389/fmars.2022.819525 (cited on page 1).

Bil, W., Zeilmaker, M., Fragki, S., Lijzen, J., Verbruggen, E., & Bokkers, B. (2020). Risk assessment of per- and polyfluoroalkyl substance mixtures: A relative potency factor approach. *Environmental Toxicology and Chemistry*, *40*(3), 859–870. https://doi.org/10.1002/etc.4835 (cited on pages 1, 5, 6).

Brusseau, M. L., & Guo, B. (2021, December). Air-water interfacial areas relevant for transport of per and poly-fluoroalkyl substances. https://doi.org/10.1016/j.watres.2021.117785 (cited on page 3).

Camporese, M., Ferraris, S., Putti, M., Salandin, P., & Teatini, P. (2006). Hydrological modeling in swelling/shrinking peat soils. *Water Resources Research*, *42*(6). https://doi.org/10.1029/2005wr004495 (cited on pages 26, 44).

Chen, D., Pyrak-Nolte, L. J., Griffin, J., & Giordano, N. J. (2007). Measurement of interfacial area per volume for drainage and imbibition. *Water Resources Research*, *43*(12). https://doi.org/10.1029/2007wr006021 (cited on page 27).

EFSA Panel on Contaminants in the Food Chain, Schrenk, D., Bignami, M., Bodin, L., Chipman, J. K., Mazo, J. del, Grasl-Kraupp, B., Hogstrand, C., Hoogenboom, L. (, Leblanc, J.-C., Nebbia, C. S., Nielsen, E., Ntzani, E., Petersen, A., Sand, S., Vleminckx, C., Wallace, H., Barregård, L., Ceccatelli, S., … Schwerdtle, T. (2020). Risk to human health related to the presence of perfluoroalkyl substances in food. *EFSA Journal*, *18*(9), 391. https://doi.org/10.2903/j.efsa.2020.6223 (cited on page 1).

Fabregat-Palau, J., Vidal, M., & Rigol, A. (2021). Modelling the sorption behaviour of perfluoroalkyl carboxylates and perfluoroalkane sulfonates in soils. *Science of The Total Environment*, *801*, 149343. https://doi.org/10.1016/j.scitotenv.2021.149343 (cited on pages 2, 5, 6, 8, 25, 29, 44).

Fetter, C. W. (2008). *Contaminant hydrogeology*. Prentice Hall. (Cited on page 44).
Freundlich, H. (1909). *Kapillarchemie*. Akademische verlagsgesellschaft m.b.h. (Cited on page 43).
Ghanbarian, B., Hunt, A. G., Bittelli, M., Tuller, M., & Arthur, E. (2021). Estimating specific surface area: Incorporating the effect of surface roughness and probing molecule size. *Soil Science Society of America Journal*, *85*(3), 534–545. https://doi.org/10.1002/saj2.20231 (cited on pages 24, 47, 53).
Grecco, H. E. (2022). *Pint: Makes units easy*. https://pint.readthedocs.io/en/stable/ (cited on page 5).
Gruijter, J. J. de, Bierkens, M. F. P., Brus, D. J., & Knotters, M. (2006). *Sampling for natural resource monitoring*. Springer Berlin Heidelberg. https://doi.org/10.1007/3-540-33161-1 (cited on page 2).
Guo, B., Zeng, J., & Brusseau, M. L. (2020). A mathematical model for the release, transport, and retention of per- and polyfluoroalkyl substances (PFAS) in the vadose zone. *Water Resources Research*, *56*(2). https://doi.org/10.1029/2019wr026667 (cited on page 2).
Guo, B., Zeng, J., Brusseau, M. L., & Zhang, Y. (2022). A screening model for quantifying PFAS leaching in the vadose zone and mass discharge to groundwater. *Advances in Water Resources*, *160*, 104102. https://doi.org/10.1016/j.advwatres.2021.104102 (cited on pages 3–8, 23, 44).
Heinen, M., Bakker, G., & Wösten, J. H. M. (2020). *Waterretentie- en doorlatendheidskarakteristieken van boven- en ondergronden in Nederland: De Staringreeks : Update 2018* (technical report Number 2978). Wageningen Environmental Research. Wageningen Environmental Research. https://doi.org/10.18174/512761 (cited on pages 4, 5, 27, 29).
Jiang, H., Guo, B., & Brusseau, M. L. (2020). Pore-scale modeling of fluid-fluid interfacial area in variably saturated porous media containing microscale surface roughness. *Water Resources Research*, *56*(1). https://doi.org/10.1029/2019wr025876 (cited on pages 3, 24, 25, 44).
KNMI. (2023a, March 16). *Bodemtemperaturen*. Retrieved March 16, 2023, from https://www.knmi.nl/nederland-nu/klimatologie/bodemtemperaturen (cited on page 28).
KNMI. (2023b, March 10). *Dagwaarden neerslagstations*. Retrieved March 10, 2023, from https://www.knmi.nl/nederland-nu/klimatologie/monv/reeksen (cited on page 27).
Krafft, M. P., & Riess, J. G. (2015). Selected physicochemical aspects of poly- and perfluoroalkylated substances relevant to performance, environment and sustainability—part one. *Chemosphere*, *129*, 4–19. https://doi.org/10.1016/j.chemosphere.2014.08.039 (cited on pages 1, 3).
Langmuir, I. (1918). The adsorption of gases on plane surfaces of glass, mica and platinum. *Journal of the American Chemical Society*, *40*(9), 1361–1403. https://doi.org/10.1021/ja02242a004 (cited on pages 3, 43, 44).

Lapré, H. (2023). *Pyfas: A wrapper around Bo Guo's PFAS LEACH screening tool*. https://doi.org/10.5281/zenodo.7739889 (cited on page 5).

Le, S., Kibbey, T. C. G., Weber, K. P., Glamore, W. C., & O'Carroll, D. M. (2021). A group-contribution model for predicting the physicochemical behavior of PFAS components for understanding environmental fate. *Science of The Total Environment*, *764*, 142882. https://doi.org/10.1016/j.scitotenv.2020.142882 (cited on pages 2, 3, 8, 25, 29, 44).

Leverett, M. (1941). Capillary behavior in porous solids. *Transactions of the AIME*, *142*(01), 152–169. https://doi.org/10.2118/941152-g (cited on page 3).

Massop, H. T. L., Bakel, P. J. T. van, Kroon, T., Kroes, J. G., Tiktak, A., & Werkman, W. (2005). *Op zoek naar de "ware" neerslag en verdamping; toetsing van de met het STONE 2.1-instrumentarium berekende verdamping aan literatuurgegevens en aan regionale waterbalansen, en de gevoeligheid van het neerslagoverschot op de uitspoeling van nutriënten* (technical report). Alterra. (Cited on pages 4, 5).

Pannu, M., & Plumlee, M. (2021, March 24). *PFAS phase I pilot-scale treatment study* (technical report). Orange County Water District. (Cited on page 25).

Paul, A. G., Jones, K. C., & Sweetman, A. J. (2008). A first global production, emission, and environmental inventory for perfluorooctane sulfonate. *Environmental Science & Technology*, *43*(2), 386–392. https://doi.org/10.1021/es802216n (cited on pages 1, 28).

Poelman, J. N. B. (1974). Dichtheid van de vaste delen van rivierkleigronden. http://edepot.wur.nl/110234 (cited on page 7).

Querner, E. P., Jansen, P. C., Akker, J. J. H. van den, & Kwakernaak, C. (2012). Analysing water level strategies to reduce soil subsidence in dutch peat meadows. *Journal of Hydrology*, *446-447*, 59–69. https://doi.org/10.1016/j.jhydrol.2012.04.029 (cited on page 26).

Rosen, M. J. (2004). *Surfactants and interfacial phenomena*. Wiley-Interscience. (Cited on pages 3, 26, 28, 43, 45).

Sha, B., Johansson, J. H., Tunved, P., Bohlin-Nizzetto, P., Cousins, I. T., & Salter, M. E. (2021). Sea spray aerosol (SSA) as a source of perfluoroalkyl acids (PFAAs) to the atmosphere: Field evidence from long-term air monitoring. *Environmental Science & Technology*, *56*(1), 228–238. https://doi.org/10.1021/acs.est.1c04277 (cited on page 28).

Silva, J. A. K., Martin, W. A., & McCray, J. E. (2021). Air-water interfacial adsorption coefficients for PFAS when present as a multi-component mixture. *Journal of Contaminant Hydrology*, *236*, 103731. https://doi.org/10.1016/j.jconhyd.2020.103731 (cited on page 2).

Silva, J. A. K., McCray, J. E., & Martin, W. A. (2019, July). *Baseline data acquisition and numerical modeling to evaluate the fate and transport of PFAS within the vadose zone. SERDP project ER18-1389* (technical report). GSI North America Inc. Retrieved September 12, 2022, from https://www.serdp-

estcp.org/projects/details/f85916e1-6a39-4ccd-b21e-210c674e1b1d/er18-1389-project-overview (cited on page 4).

Silva, J. A. K., Šimůnek, J., & McCray, J. E. (2022). Comparison of methods to estimate air-water interfacial areas for evaluating PFAS transport in the vadose zone. *Journal of Contaminant Hydrology*, *247*, 103984. https://doi.org/10.1016/j.jconhyd.2022.103984 (cited on pages 2, 3, 8, 23, 24, 47–51, 54).

U.S. EPA. (2022a, June). *Drinking water health advisory: Hexafluoropropylene oxide (HFPO) dimer acid (CASRN 13252-13-6) and HFPO dimer acid ammonium salt (CASRN 62037-80-3), also known as "GenX chemicals"* (technical report) (EPA/822/R-22/005). U.S. Environmental Protection Agency. (Cited on pages 25, 29).

U.S. EPA. (2022b, June). *Drinking water health advisory: Perfluorobutane sulfonic acid (CASRN 375-73-5) and related compound potassium perfluorobutane sulfonate (CASRN 29420-49-3)* (technical report) (EPA/822/R-22/006). U.S. Environmental Protection Agency. (Cited on pages 25, 29).

Verburg, P. H. (1995). *De relatie tussen de vochttoestand van de bodem en de vochtindicatie van de vegetatie: Een nadere bepaling van de grens tussen 'vochtig' en 'droog' binnen het ecotopensysteem* (technical report). Landbouwuniversiteit Wageningen. (Cited on page 28).

Vereecken, H., Weynants, M., Javaux, M., Pachepsky, Y., Schaap, M. G., & Genuchten, M. T. van. (2010). Using pedotransfer functions to estimate the Van Genuchten-Mualem soil hydraulic properties: A review. *Vadose Zone Journal*, *9*(4), 795–820. https://doi.org/10.2136/vzj2010.0045 (cited on page 2).

Verschragen, P. (2019, December 19). *Verkennend bodemonderzoek naar PFAS inclusief GenX op diverse terreinen van NS Vastgoed rond afvalverbrandingscentrales* (technical report). Aveco de Bondt. Holten. (Cited on page 28).

Vogel, H.-J., Hoffmann, H., & Roth, K. (2005). Studies of crack dynamics in clay soil: I. experimental methods, results, and morphological quantification. *Geoderma*, *125*(3-4), 203–211. https://doi.org/10.1016/j.geoderma.2004.07.009 (cited on page 27).

Wang, Y., Khan, N., Huang, D., Carroll, K. C., & Brusseau, M. L. (2021). Transport of PFOS in aquifer sediment: Transport behavior and a distributed-sorption model. *Science of The Total Environment*, *779*, 146444. https://doi.org/10.1016/j.scitotenv.2021.146444 (cited on pages 4, 44).

Wintersen, A., Claessens, J., Wit, M., Helvoort, K. van, Wolters, M., Stoffelsen, B., Wijnen, H. van, & Breemen, P. van. (2021). Landsdekkend beeld van PFAS in Nederlands grondwater. https://doi.org/10.21945/RIVM-2021-0205 (cited on page 28).

Xu, M., & Eckstein, Y. (1995). Use of weighted least-squares method in evaluation of the relationship between dispersivity and field scale. *Ground Water*, *33*(6), 905–908. https://doi.org/10.1111/j.1745-6584.1995.tb00035.x (cited on page 8).

Appendices

Appendix A

Model parameters

A.1 Soil composition

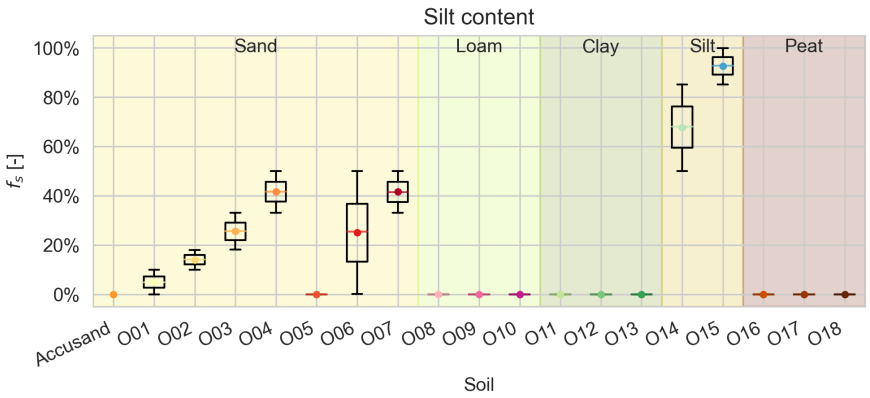

Figure A.1: Distribution of the silt content of the different Staring soils.

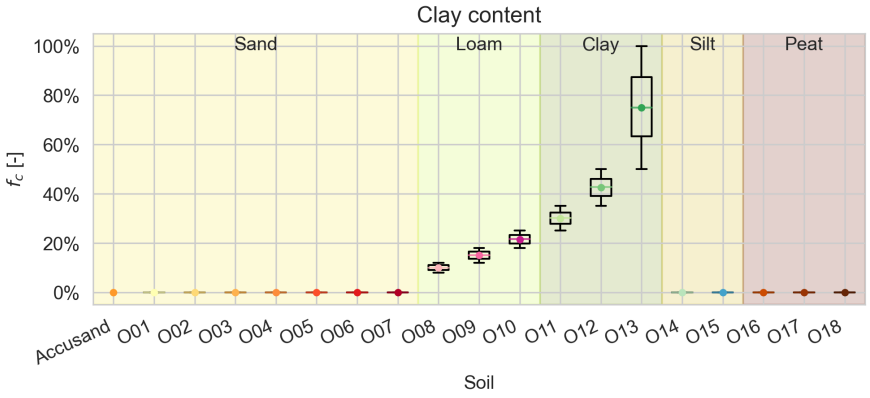

Figure A.2: Distribution of the clay content of the different Staring soils.

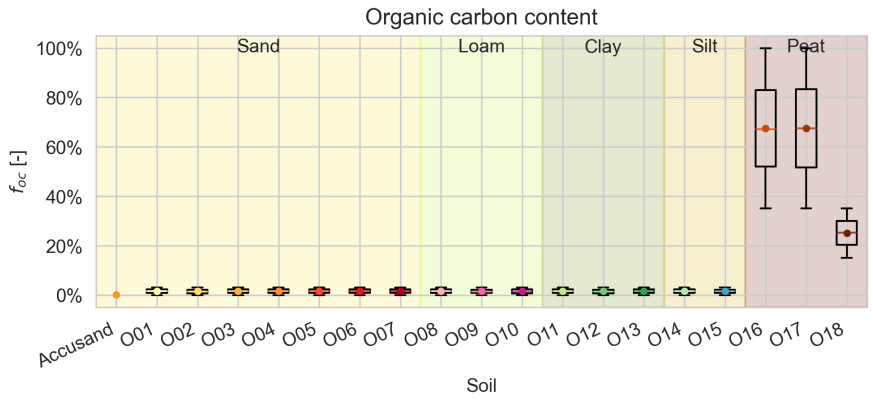

Figure A.3: Distribution of the organic matter content of the different Staring soils.

A.2 Soil water content

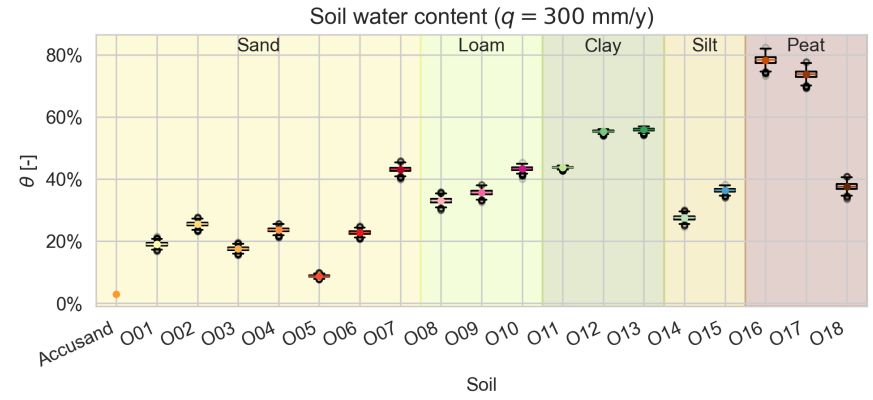

Figure A.4: Distribution of the water content of the different Staring soils.

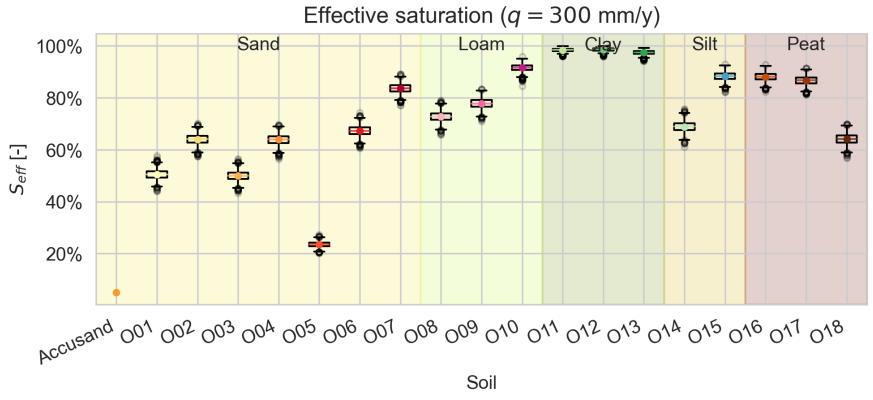

Figure A.5: Distribution of the effective water saturation of the different Staring soils.

A.3 Derived parameters

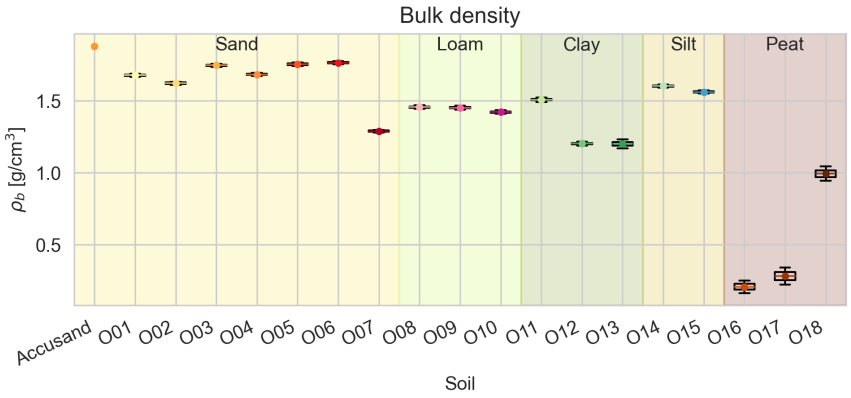

Figure A.6: Distribution of the bulk density of the different Staring soils.

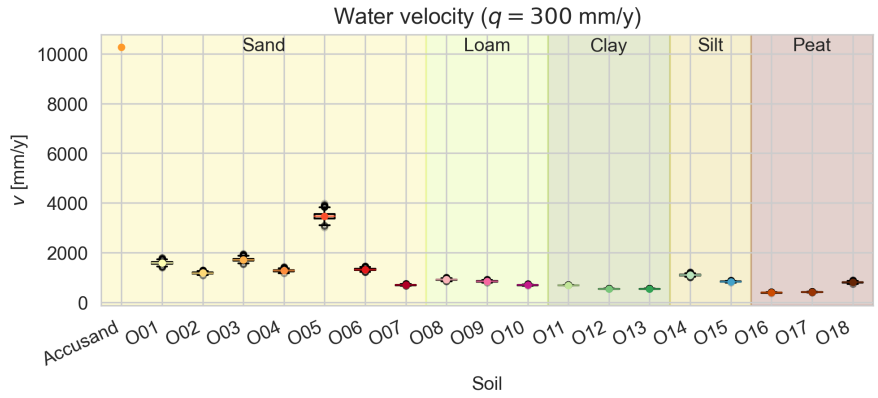

Figure A.7: Distribution of the water velocity of the different Staring soils.

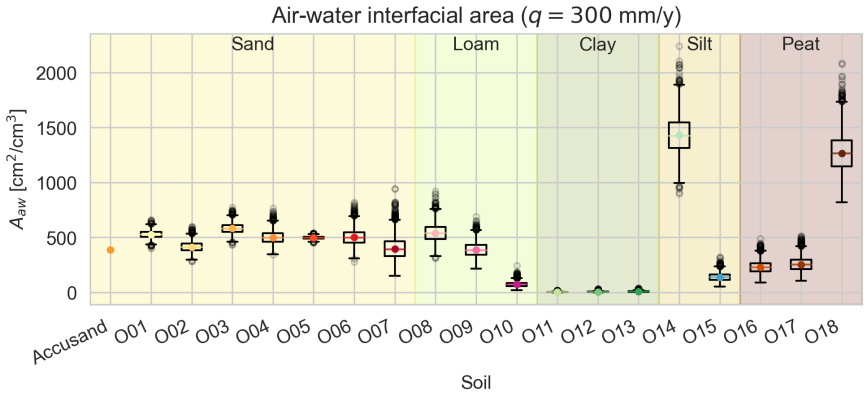

Figure A.8: Distribution of the air-water interfacial area of the different Staring soils.

Appendix B

Adsorption from the water phase to interfaces with solids and air

Adsorption to solid-water interfaces is often described in terms of a partitioning coefficient, K_d, which represents the ratio between the water dissolved concentration of a substance and the adsorbed concentration. In contrast, the sorption to AWIs is described as a function of the surface area per unit volume, A_{aw}, and the surface excess concentration, Γ. As shown below, these are equivalent under the assumption that the specific surface area of the soil remains constant.

In its most generic form adsorption to an interface can be calculated as:

$$C_i = A_i(\theta) \cdot \Gamma_i \left(C_{aq}\right), \tag{B.1}$$

where C_i is the concentration on the interface in per unit volume of porous medium, A_i is the specific surface area of the porous medium, and Γ_i is the surface excess concentration per unit area of interface as a function of the aqueous concentration C_{aq} per unit volume of pore water. The surface excess concentration is the increase in concentration of the substance in the interface compared to the concentration in the bulk pore water. (Rosen, 2004) Various models for Γ_i exist, called isotherms, such as the Freundlich isotherm (Freundlich, 1909):

$$\Gamma_i(C_{aq}) = \kappa_i \cdot C_{aq}^N, \tag{B.2}$$

with a sorption coefficient κ_i and a shape parameter N. For $N = 1$ this reduces to a linear model. A second model is the Langmuir isotherm, which is derived from the dynamic equilibrium between adsorption and desorption (Langmuir, 1918):

$$\Gamma_i(C_{aq}) = \Gamma_{max} \frac{\kappa_i \cdot C_{aq}}{1 + \kappa_i \cdot C_{aq}}, \tag{B.3}$$

with Γ_{max} the physical maximum surface excess concentration.

B.1 Solid-water interfaces

For solid-water interfaces the surface excess concentration is more commonly written in terms of the adsorbed mass per unit mass of porous medium, by dividing the equation for C_i by the bulk density ρ_b. For most soils the interfacial area is a constant, and is therefore often included in the partitioning coefficient. This also means that this simplification is not allowed for peat soils, as these soils tend to swell and shrink with changing moisture content (Camporese et al., 2006). As an example, for the Freundlich isotherm the Freundlich isotherm for solid-water interfacial adsorption becomes (Fetter, 2008):

$$C_s = \frac{A_i \kappa_i}{\rho_b} \cdot C_{aq}^N = K_d C_{aq}^N. \tag{B.4}$$

Natural soils contain a mixture of different materials, which all have different adsorption characteristics. In that case the total sorption is a linear combination of the individual sorption characteristics (Langmuir, 1918):

$$C_s = C_{aq} \sum_k^n \left(f_k K_k(C_{aq}) \right), \tag{B.5}$$

where $k..n$ is the index of the different soil materials, f_k is the fraction of soil consisting of material k, and $K_k(C_{aq})$ is the partitioning coefficient of the material at a given aqueous concentration. This property can be used to estimate the adsorptive properties of PFASs using the composition of the soil and partitioning coefficients of the constituents. These coefficients can be obtained from measurements for the specific PFAS in the individual soil components (Wang et al., 2021) or by estimating the properties from the molecular structure (Fabregat-Palau et al., 2021; Le et al., 2021). From these models it is clear that the organic matter has the highest potential for adsorption, but clay and silt minerals, as well as metal oxides play an important role in the adsorption of PFAS.

B.2 Air-water interfaces

For AWI the A_{aw} is heavily dependent on the soil moisture content (Jiang et al., 2020), and therefore combining the simplification of including the A_{aw} in the partitioning coefficient is not valid. Also, as the Langmuir isotherm is based on the equilibrium between the physical adsorption and desorption rates for a single type of sorption site; and the AWI contains a single type of sorption site, the sorption to these interfaces is accurately described by the Langmuir isotherm (Guo et al., 2022; Langmuir, 1918):

$$\Gamma_{aw} = \Gamma_{max} \frac{K_{eq} \cdot C_{aq}}{1 + K_{eq} \cdot C_{aq}} \tag{B.6}$$

Combining Equation B.1 and Equation B.6 gives Equation 1.5:

$$C_{aw} = A_{aw} \cdot \Gamma_{aw} = A_{aw} \cdot \Gamma_{max} \frac{K_{eq} \cdot C_{aq}}{1 + K_{eq} \cdot C_{aq}} \tag{B.7}$$

B.3 Environmental conditions

It is important to note that in all isotherms the sorption coefficient κ_i and the maximum surface excess concentration Γ_{max} are presented as constants, while in reality they are a function of various environmental parameters, such as temperature, pH, and the concentration of other substances in the pore water. No model exists that can describe the dependence of κ_i and Γ_{max} on all these parameters simultaneously. However, some general notes on the maximum sorption, Γ_m, are given by Rosen (2004):

- Γ_m increases with longer chains of CF_x up to a chain length of approximately 10, and beyond a chain length of about 16 it decreases due to coiling of the chains, which causes the molecules to occupy more surface area.
- Γ_m increases for ionic PFASs with the addition of electrolyte due to a decrease in electrostatic repulsion between the hydrophilic heads in the surface monolayer.
- Γ_m decreases with increasing temperature, attributed to increased thermal motion of the molecules.

Appendix C

Surface Roughness Multiplier (SRM)

Silva et al. (2022) compared multiple measurement techniques as well as estimations using the Leverett thermodynamic model (LTM) for the air-water interfacial area. As the aqueous tracer measurements appear to be most representative of the A_{aw} available for adsorption, and those measurements in all cases produce higher values than the estimates from the LTM, they suggest adding a Surface Roughness Multiplier (SRM) to the LTM to fit the measurements. The suggested method uses the Soil Surface Roughness Factor (SRF) as a proxy for the roughness of the air-water interfaces. Silva et al. (2022) suggest to use the slope of the relationship between the SRF and the Surface Fractal Dimension (D_s) (Ghanbarian et al., 2021) to estimate the slope of the SRM. The justification for this relationship is to be found in Figure 4a of the paper, reproduced below (Figure C.1a). From this figure it is not clear there is a strong relationship between the variables, and the corresponding Pearson correlation coefficient, R^2, is not published. When reproducing the figure with the data from the paper including the R^2, it is clear that the relationship is non-existent, given an $R^2 = 0.078$ (Figure C.1b).

Silva et al. (2022) report that the slope between D_s and SRF is used to extrapolate the data for the SRM, which should be shown in Figure 4b of the paper (reproduced in Figure C.2). In that figure an equation is shown that should describe the SRM. However, in the paper it is also reported that this model needs to be scaled in order to get an SRM of 1 for smooth surfaces (SRF $= 1$), but it is not clear how it is scaled, or why no factor is included in the equation in the first place to accomplish this. When multiplying the equation in Figure 4b by the factor of $\frac{1+2.5}{0.0875} = 40$, the SRM at SRF $= 1$ is indeed 1, but at SRF $= 1000$ the SRM is still only 1.4 and not close to 3.4, as suggested by Figure C.2.

Silva et al. (2022) include values for the SRM in Table 2 (Figure C.4) of their paper. These values cannot be reproduced from the proposed model in the paper. However, the plotted relationship in Figure C.2 strongly resembles a logarithmic model instead of the reported linear model. Plotting the values from Table 2 against the natural logarithm of the SRF shows two distinct lines of points (Figure C.3).

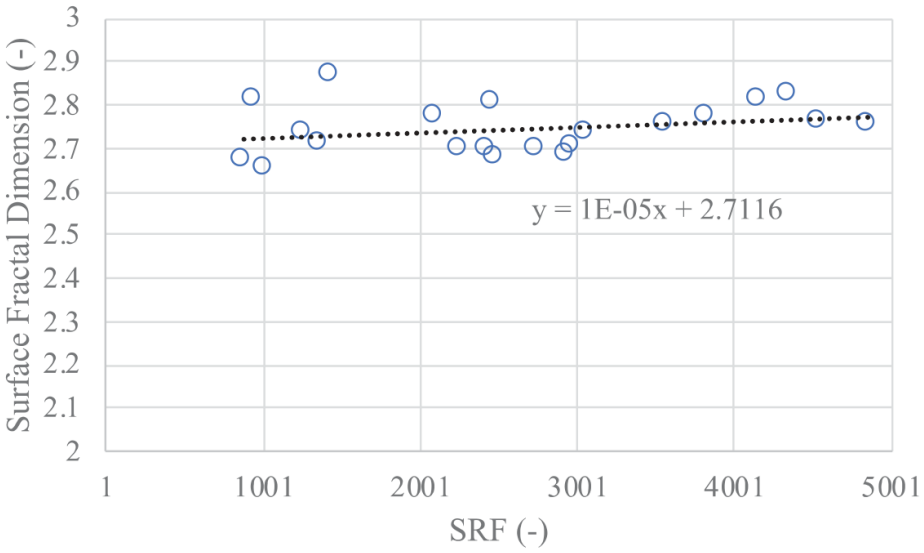

(a) Original Figure 4a as published by Silva et al. (2022)

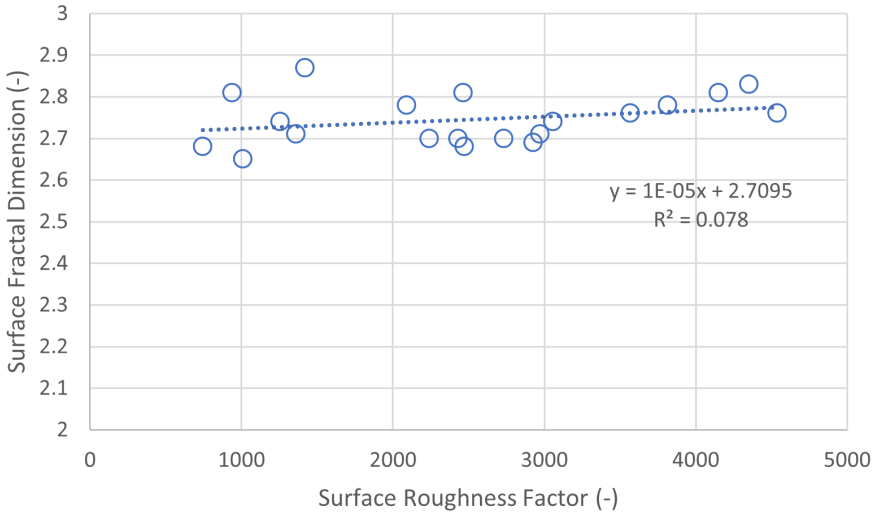

(b) Reproduction including R^2

Figure C.1: Relationship between the D_s and SRF.

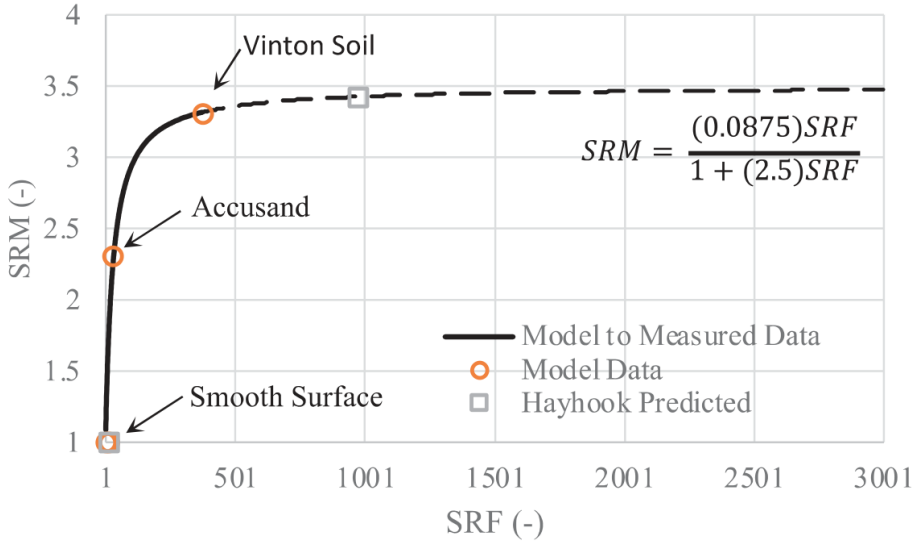

Figure C.2: Proposed relationship between SRM and SRF (Figure 4b by Silva et al. (2022)).

The first 6 soils in Figure C.4 are represented by the orange dots, with $R^2 = 0.972$, and the remaining soils are represented by the blue dots, with $R^2 = 1$, suggesting that two separate logarithmic models were employed to produce the reported data. From the paper it is unclear why there should be two distinct lines at all, especially given the fact that two very similar soils (#6 and #8) are in two different clusters.

Apart from the fact that the proposed model does not fit the data, the paper

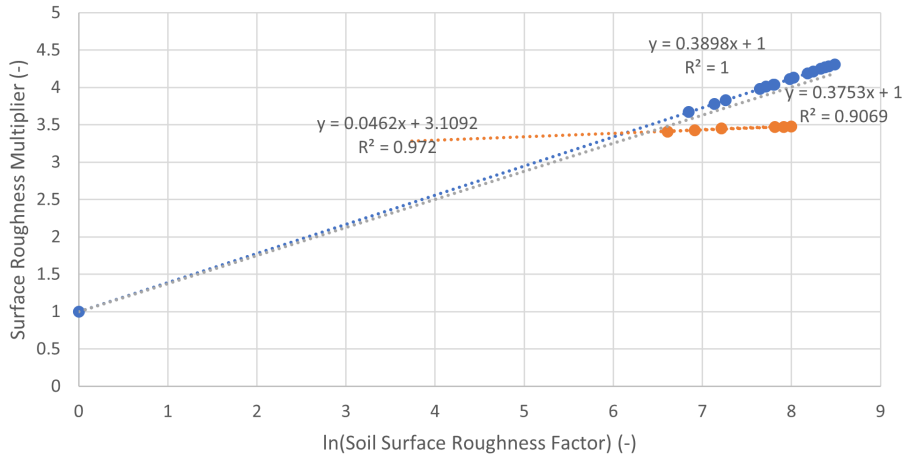

Figure C.3: SRM values from Table 2 against the natural logarithm of the SRF.

Table 2
Soil properties data used to modify LTM prediction.

Arizona soils	SSA_{BET}[a] (cm^{-1})	Category	%sand/silt/clay	porosity	d_{50} (mm)	GSA (cm^{-1})	SRF	SRM	D_s (–)
1	22,800	sand	91/7/2	0.36	0.17	22.6	1009	3.43	2.65
2	16,800	sand	96/3/1	0.36	0.17	22.6	744	3.41	2.68
3	37,500	loamy sand	81/14/5	0.38	0.135	27.6	1361	3.45	2.71
4	93,750	sandy loam	74/18/8	0.38	0.098	38.0	2470	3.47	2.68
5	76,500	loamy sand	80/14/6	0.37	0.135	28.0	2732	3.47	2.70
6	111,000	sandy loam	67/25/8	0.39	0.098	37.3	2972	3.48	2.71
7	296,100	sandy loam	71/16/13	0.39	0.06	61.0	4854	4.31	2.76
8	107,550	sandy loam	59/32/9	0.4	0.098	36.7	2928	4.11	2.69
9	149,400	sandy clay loam	53/26/21	0.43	0.07	48.9	3058	4.13	2.74
10	150,750	silt loam	22/53/25	0.46	0.027	120.0	1256	3.78	2.74
11	222,900	loam	37/46/17	0.42	0.035	99.4	2242	4.01	2.70
12	466,800	loam	39/40/21	0.4	0.035	102.9	4538	4.28	2.76
13	392,550	sandy clay loam	66/15/27	0.4	0.035	102.9	3816	4.21	2.78
14	317,700	sandy clay loam	58/15/27	0.42	0.027	128.9	2465	4.04	2.81
15	525,600	sandy clay loam	51/22/27	0.43	0.027	126.7	4149	4.25	2.81
16	436,050	silt loam	4/73/23	0.45	0.027	122.2	3568	4.19	2.76
17	397,050	clay loam	26/45/29	0.43	0.018	190.0	2090	3.98	2.78
18	535,200	silty clay	9/40/51	0.43	0.006	570.0	939	3.67	2.81
19	781,500	clay	29/19/52	0.45	0.006	550.0	1421	3.83	2.87
20	570,750	sandy clay loam	49/21/30	0.41	0.027	131.1	4353	4.27	2.83
21	92,250	sandy loam	71/20/9	0.38	0.098	38.0	2430	4.04	2.70

[a] Reported specific surface area from N_2/BET. d_{50} values from Dosskey et al. (2006). D_s is the surface fractal dimension (Ghanbarian et al., 2021).

Figure C.4: Soil properties used to modify the SRM (Table 2 by Silva et al., 2022).

by Silva et al. (2022) does provide a good overview of the different measurement techniques and their applicability. Also, the concept of using a model for the soil roughness to modify the LTM appears to be well justified, unfortunately the reported model is severely flawed, to the point of uselessness. It is therefore recommended that more measurements are taken of the A_{aw} on a wide range of natural soils and under different soil moisture conditions, and more research should be done to find a better model for the SRM.

Glossary

A_{aw}**:** air-water interfacial area.

AWI: air-water interface.

D_s**:** Surface Fractal Dimension, a measure of the surface roughness of the soil (Ghanbarian et al., 2021). When $D_s = 2$ the surface is perfectly smooth, while $D_s = 3$ indicates an extremely rough surface.

EFSA: European Food Safety Authority.

HFPO-DA: Hexafluoropropylene oxide dimer acid, a branched PFAS with a tail length of 5 and carbonic acid as its head.

Chemical formula: $CF_3(CF_2)_2 - O - CF(CF_3)COOH$.

LTM: Leverett thermodynamic model.

PFAS: per- and polyfluoroalkyl substance.

PFBA: Perfluorobutanoic acid, a PFAS with a tail length of 3 and carbonic acid as its head.

Chemical formula: $CF_3(CF_2)_2COOH$.

PFBS: Perfluorobutane sulfonic acid, a PFAS with a tail length of 4 and sulfonic acid as its head.

Chemical formula: $CF_3(CF_2)_3SO_3H$.

PFDA: Perfluorodecanoic acid, a PFAS with a tail length of 9 and carbonic acid as its head.

Chemical formula: $CF_3(CF_2)_8COOH$.

PFHpA: Perfluoroheptanoic acid, a PFAS with a tail length of 6 and carbonic acid as its head.

Chemical formula: $CF_3(CF_2)_5COOH$.

PFHxA: Perfluorohexanoic acid, a PFAS with a tail length of 5 and carbonic acid as its head.

Chemical formula: $CF_3(CF_2)_4COOH$.

PFHxS: Perfluorohexane sulfonic acid, a PFAS with a tail length of 6 and sulfonic acid as its head.

Chemical formula: $CF_3(CF_2)_5SO_3H$.

PFNA: Perfluorononanoic acid, a PFAS with a tail length of 8 and carbonic acid as its head.

Chemical formula: $CF_3(CF_2)_7COOH$.

PFOA: Perfluorooctanoic acid, a PFAS with a tail length of 7 and carbonic acid as its head.

Chemical formula: $CF_3(CF_2)_6COOH$.

PFOS: Perfluorooctane sulfonic acid, a PFAS with a tail length of 8 and sulfonic acid as its head.

Chemical formula: $CF_3(CF_2)_7SO_3H$.

PFPeA: Perfluoropentanoic acid, a PFAS with a tail length of 4 and carbonic acid as its head.

Chemical formula: $CF_3(CF_2)_3COOH$.

RIVM: National Institute for Public Health and the Environment.

SRF: Soil Surface Roughness Factor, a measure of the surface roughness of the soil particles.

SRM: Surface Roughness Multiplier, an empirical factor to compensate for the underestimation of the air-water surface area by the Leverett thermodynamic model when compared to measurements in the same soil (Silva et al., 2022).

SWI: solid-water interface.

TFA: Trifluoroacetic acid, a PFAS with a tail length of 1 and carbonic acid as its head.

Chemical formula: CF_3COOH.